Machine Learning, Probabilistic and Mathematical Models for

Damage Recognition in Structural Systems

BY

EBRAHIM NAZARIAN
M.Sc., University of Illinois at Chicago, Chicago, IL, 2017
B.S., Budapest University of Technology and Economics, Budapest, Hungary, 2012

THESIS

Submitted as partial fulfillment of the requirements
for the degree of Doctor of Philosophy in Civil Engineering
in the Graduate College of the
University of Illinois at Chicago, 2017

Chicago, Illinois

Defense Committee:

        Farhad Ansari, Chair and Advisor
        Didem Ozevin
        Eduard Karpov
        Michael Pagano, Public Administration
        Sheng-Wei Chi

ACKNOWLEDGEMENTS

I would like thank my advisor, Prof. Farhad Ansari, for his support and patient throughout my entire PhD program. Prof. Ansari's experience and leadership throughout the past years gave me the ability to think independently and come with original ideas to advance my research. This thesis would not have been possible without his consistent guidance and support.

I would like thank my review committee, Dr. Didem Ozevin, Dr. Eduard Karpov, Dr. Michael Pagano and Dr. Sheng-Wei Chi, for the time that they have spent on reviewing my thesis and their suggestions to improve this thesis. Furthermore, I would like to thank my fellow researchers, Dr. Ander Zornoza, Dr. Dewei Meng, Mr. Elias Oskoui, Ms. Fereshteh Sabet, Dr. Saeed Babanejad for their continuous support and help throughout my thesis, Dr. Xiaotan Zhang for designing the scaled model of the cable-stayed bridge, Mr. Todd Taylor for construction of the cable-stayed bridge and tests on the building, and Dr. Weifeng Tian for collaboration on the building project.

Contribution of Authors

With permission from ASCE (American Society of Civil Engineers), the content of the published manuscript, "Nazarian E, Ansari F, Zhang X, Taylor T (2016) Detection of Tension Loss in Cables of Cable-Stayed Bridges by Distributed Monitoring of Bridge Deck Strains. Journal of Structural Engineering, 142(6), 04016018", is used in this thesis, in which I was the main driver of the research and the primary author of the manuscript. Dr. Farhad Ansari contributed in writing of the manuscript and guiding me during the research, Dr. Xiaotan Zhang contributed in designing the scaled model of the cable-stayed bridge, Mr. Todd Taylor contributed in construction of the scaled cable-stayed bridge.

Additionally, the materials published in the publication "Nazarian E, Ansari F, Azari H (2015). Recursive optimization method for monitoring of tension loss in cables of cable-stayed bridges. Journal of Intelligent Material Systems and Structures, 1045389X15620043" is also reused in this thesis with permission, in which I was also the main author and the primary driver of the research. In a similar manner, Dr. Farhad Ansari contributed in writing of the manuscript and guiding me during the research project. and Dr. Hoda Azari contributed in revising the manuscript.

TABLE OF CONTENTS

LIST OF TABLES

LIST OF FIGURES

SUMMARY

An increasing percentage of building and bridge structures across United States are exceeding their design life. Ensuring the structural integrity of such structures demands health monitoring strategies. Fiber optic and electrical technologies are effective tools to monitor the structural displacement and material strains. Development of these sensing technologies in the recent years has equipped the structural health monitoring field with distributed and real time sensing tools. In this research, I have developed mathematical methodologies to determine structural damages based on such sensing tools in cable-stayed and building structures.

Cables of cable-stayed bridges play a critical role in cable-stayed bridges by transmitting the forces from the bridge deck to the pylons. Hence, assurance of integrity of the cables during the design life of the bridge is inevitable. I have developed two mathematical methodologies for detection and quantification of damage in cable-stayed structures.

The first method uses the distributed measurement of strains along the bridge deck to detect the cables that have totally or partially lost their tensile force. The fundamental principle employed in formulating the method is the interrelationship between the individual cable forces and the bending moment along the bridge span. The efficiency of the methodology was evaluated through both numerical simulations and experimentations on a reduced-scale cable-stayed bridge. Experimental results revealed that this method was capable of detecting the cables that had experienced tension losses of 30% or more.

The second proposed approach utilizes point-style sensors to estimate the deck element shear forces adjacent to the supports. An analytical approach was developed to quantify the damage in the cables using the shear forces. The formulations are based on a recursive

optimization technique, in which model updating is employed to account for the changes in the cable stiffness as a result of damage.

Furthermore, the current research proposes a hybrid approach based on machine learning models and implementation of loads tests to determine damages in the structural elements of building structures. The implemented machine learning methods in this thesis are Support Vector Machines, Neural Networks and Gaussian Naïve Bayes. The efficiency of the proposed approach was evaluated through numerical simulations and actual experimentations on a six-story heritage timber-masonry building.

1. INTRODUCTION

The content of this chapter was published as "Nazarian E, Ansari F, Zhang X, Taylor T (2016) Detection of Tension Loss in Cables of Cable-Stayed Bridges by Distributed Monitoring of Bridge Deck Strains. Journal of Structural Engineering, 142(6), 04016018" and "Nazarian E, Ansari F, Azari H (2015). Recursive optimization method for monitoring of tension loss in cables of cable-stayed bridges. Journal of Intelligent Material Systems and Structures, 1045389X15620043". Reproduced with permission from ASCE and Journal of Intelligent Material Systems and Structures.

1.1. Background

According to the Federal Highway Administration agency (FHWA), increasing portion of structures in the United States are exceeding their design life, As a result, ensuring the safety of these structures is a very important task. Over the past years, various structural health monitoring approaches have been developed for detection of the intensity and the location of damages in various structures such as building and bridges. Advancements in structural health monitoring rely on development of sensors and development of mathematical approaches that can interpret the sensor data to meaningful information about the health of the structure. Current structural health monitoring solutions target different applications and they have their own limitations and advantages.

For instance, in case of a cable-stayed bridges, health-state of the cable stays is important because cables play a critical role by transmitting the forces from the deck to the pylons. These cables represent a considerable portion of the investment in such bridges because approximately 25% of the construction cost is expended on the cables. Replacement of damaged stay cables costs more than the original cost of the cables at the time of

construction (Li et al. 2011). Stay cables are prone to deterioration and damage due to fatigue, and corrosion (Mehrabi 2006; Sun et al. 2013). As a result, inspection and monitoring becomes important in consideration of the importance of cables within the structural system.

Current approaches in health monitoring of cable-stayed bridges include both global and localized methods. Changes in cable forces provide indications about either loss in global cable stiffness or due to the displacements of individual cables, i.e. bond in anchorages, or cable deformations. Computational approaches have been primarily based on global vibration response of bridges. They lack sufficient resolution for health monitoring of the cable-stays (Talebinejad et al. 2011). Localized nondestructive test (NDT) methods have been developed either for specific use in monitoring the cable forces or adapted from the existing technologies for damage assessment. For instance, magnetic flux leakage has been employed for measuring the stress in cables (Kim and Park 2007; Li et al. 2011). This approach requires field calibrations with identical cables in order to determine the relationship between magnetic permeability and strain in the cables. The method is vulnerable to temperature and proximity to electromagnetic fields (Kim and Park 2007; Christen et al. 2003; Sun et al. 2013). Another approach pertains to the measurement of cable forces based on the fundamental vibration frequency of cables. Use of this technique is limited to long cables. Measurement precisions for short cables are low due to boundary condition uncertainties, and geometrical constraints (Russell and Lardner 1998; Ren et al.

2005; Lanza di Escala et al. 2003). Discrete sensors such as fiber Bragg Gratings (FBG) have proven to be unreliable when embedded inside of the cables for new bridges (Li et al. 2011; Li et al. 2009). Embedded sensors often fail either right after embedment within the strands or shortly thereafter. In order to overcome the bare FBG shortcomings, Li et al. (2011) introduced the FBG-FRP smart cable, which uses high durability glass fibers for embedment of the FBG sensors. Smart cables have the potential for widespread usage, once issues pertaining to the long-term survivability of the FBGs within the cable system and replacement costs are resolved. Large numbers of externally attached strain and acceleration-based sensors are required for effective monitoring of all the cables within these bridges. Externally attached sensors to the cables are primarily applicable for the cables that do not require protective casings. The method based on image processing has shown to be effective in application to a cable stayed bridge (Kim et al. 2013). The applicability of the method is limited to favorable weather conditions since the acquired images require proper lighting to achieve high resolutions. In general, use of many discrete sensors either embedded or attached requires processing of large volumes of data. In such cases, the accumulated data requires enormous amounts of time for post processing activities (Mehrabi 2006; Fricker and Vogel 2007; Christen et al. 2003; Kang et al. 2009).

In a similar manner to cable-stayed bridges, various localized and global structural health monitoring techniques have been implemented for damage detection in building structures. Investigation of the dynamic properties of the buildings has been the primary approach in

global damage assessment of such structures. A number of researchers have developed computational approaches to interpret structural damage from the dynamic properties. Modal frequency is one of the popular methods in dynamic assessment of damage in structural systems (Ren et al. 2002; Stubbs et al. 1990; Stubbs et al. 1996). For instance, Soyoz (2012) studied vibration response of a reinforced-concrete building before and after retrofitting by both ambient and forced-vibration techniques. The results showed that the modal frequency increased after retrofitting. Despite the popularity of the modal frequency approach in damage detection, it is realized that this approach can detect only moderate to larger levels of damage (Cao et al, 2016). Mode-shape method is another dynamic based approach have been extensively studied. Mode shapes can detect lower intensities of damage compare to the modal frequency approaches (Cao et al, 2016). However, determination of mode shapes requires significant number of sensors on the structure (Abeykoon et al, 2015). Measurement of damping is another dynamic based method for assessment of the structural behavior (Zarafshan et al, 2014). Even though damping plays an important role in structural health monitoring, uncertainty in damping measurements has been a drawback and it has been an on-going research topic. The uncertainties are due to inherent complexity of damping mechanism, lack of a generalized mathematical model, and difficulties in experimental implementations of the method (Cao et al, 2016). In general, structural dynamic based methods have been more successful for damage assessment of slender structures.

An example of localized approaches used for assessment of damage in building structures include ultrasonic pulse velocity (UPV). This technology determines the quality of various construction materials by measuring the sonic wave velocity in the material (Shaji et al. 2000; Dilek et al. 2007). This method has sources of uncertainty due to the moisture content, transducer contact with the material, and influence of reinforcement (Bungey 1980). Another example is the application of the widely used rebound hammer. This technology estimates the strength of materials, mainly concrete and rock, by measuring the rebound of a spring-loaded mass striking the material surface (Gorokhovich, 2010). Application of this device is influenced by the hardness of the impact point. Thus, the results of the rebound hammer do not reflect information on the overall strength of the structural component. In general, use of localized nondestructive testing methods is limited to the condition of the material within a small region rather than the overall stiffness of the structural component.

Crack detection and monitoring is another common approach in monitoring the health-state of a structure. Cracking can be caused by various reasons such as aging or foundation settlements. In monitoring of the large structures, often a series of sensors are installed throughout the structure to monitor the overall structural behaviour. Traditionally, the sensors were connected to the processing unit through a wired communication. However, as the result of developments in wireless communications in the recent years, wireless network of sensors can be implemented to employ a large number of sensors along the

entire structure (Potenza et al, 2015). Even though such network of sensors can be implemented to study the overall condition of the structure with convenience, monitoring the crack development does not provide information about existing condition of the structure, rather it provides insight about the changes in the structure after the installation of the sensors.

In structural health monitoring of heritage structures which commonly involve masonry elements, acoustic emission (AE) technique can be used to determine the extent of damage using the energy released during the crack propogation. The efficiency of this approach was evaluated by Carpinteri et al (2005) through implementation in a heritage structure in Italy. This method requires signals at the time that the material is subject to damage, hence this approach can not be implemented to assess damages of structures with existing damages.

1.2. Research Objective

The objective of this research is to develop theoretical approaches, based on machine learning and mathematical models, to recognize damages in the cable-stayed and building structures using strain sensors data. Three different theoretical solutions were proposed in this thesis to advance structural health monitoring solutions in cable-stayed and building structures.

The first proposed solution addresses detection of damage in cable-stayed bridges using distributed sensing. In this case, the objective was to develop a method for quantifying the forces in the cables and detecting the support reactions of single plane cable stayed bridges by measuring the distributed strains along the lengths of bridge spans. The analytical formulations established here are based on the premise that the distribution of strain along the length of the deck is influenced by changes in the amplitudes of the discrete forces exerted by the cables. The proposed approach will enable monitoring the change in cable forces by measurement of the deck strains alone, and therefore, eliminates the need for attaching sensors to the cables of the bridges. Distributed sensing by Brillouin scattering has been thoroughly detailed in the technical literature. It is briefly described next for completeness, followed by the description of the proposed analytical method, and experimentation by using a scaled model of a cable stayed bridge in the laboratory.

The objective of the second proposed solution was to determine deficiency in the cables of cable stayed bridges by determining the support shear forces using point-style sensors. Cable-stayed bridges are typically mid to long span structures in which the primary load paths of the structural system (bridge deck) provide important information about the condition state of the secondary structural elements (stay cables). For instance, changes in the cable forces result in changes in the bridge deck strains. In this case, damage in the cables of cable-stayed bridges results in a reduction of the tensile forces in the cables. Hence, a significant portion of loss in the cable forces is transmitted to the supports, and

as change in internal shear forces in interior sections along the span. The work described in this thesis employs a new method that utilizes the change in support reactions to detect the location and intensity of the damage in the stay cables. To increase accuracy in quantification of damage in cable stays, more sensors can be employed along the deck in order to incorporate the effect of deck elements shear as well as the support reactions. The proposed analytical approach is formulated as an optimization problem by minimizing the difference of measured damage response and the theoretical response. This approach eliminates the necessity for attaching sensors on the cables, and it will enable monitoring the change in cable forces utilizing the support reactions only.

The third proposed solution pertains to development of a theoretical approach to detect damage in the building structures using point-style sensors. The change in stiffness of structural systems is an indication of damage, and the magnitude and distribution of strain within the structure is affected by change in the stiffness of elements. Hence, monitoring the strain in structural members can provide information about their integrity. The objective of in this case study, is to develop a hybrid approach for detection and quantification of damage in structural systems by means of machine learning (ML) models and load tests on selected frames within a structural system. The structure under study for the experimental evaluation is a historical six-story timber frame masonry building that experienced severe damage due to differential settlement of its foundation. Herein, we will first establish the robustness of the ML model through numerical simulation using finite element modelling

(FEM), and then we show the effectiveness of the method through actual experimentation on selected frames of a large structure. The methodology described herein examines the application of three different machine learning (ML) techniques for determination of stiffness loss in structural components, namely: Support Vector Machines (SVM), Neural Networks (NN), and Gaussian Naïve Bayes (GNB). These methods are explained in detail in the literature, and they have been concisely explained in the following sections of this thesis for completeness.

CHAPTER 2

2. THEORETICAL APPROACH

The content of this chapter was published as "Nazarian E, Ansari F, Zhang X, Taylor T (2016) Detection of Tension Loss in Cables of Cable-Stayed Bridges by Distributed Monitoring of Bridge Deck Strains. Journal of Structural Engineering, 142(6), 04016018" and "Nazarian E, Ansari F, Azari H (2015). Recursive optimization method for monitoring of tension loss in cables of cable-stayed bridges. Journal of Intelligent Material Systems and Structures, 1045389X15620043". Reproduced with permission from ASCE and Journal of Intelligent Material Systems and Structures.

In this chapter, the theoretical approach for interpreting damage in each of the three cases mentioned in the introduction chapter are illustrated. As explained in the introduction chapter, the mathematical formulations of the first and second proposed methods pertain to detection of damage in the cables of cable-stayed bridges using distributed and point-style strain sensors, respectively. In both these two approaches, mathematical optimization techniques are the fundamental principle of the analytical formulations. In the third proposed method, the analytical formulations utilize machine learning techniques for detection of damage in building structures.

2.1. Constrained Optimization Approach Using Distributed Strain Sensing

2.1.1. Brillouin Scattering Based Measurement of Distributed Strains

Over the past two decades, distributed sensing using Brillouin scattering has been actively

employed in oil and gas exploration activities (Bao 2009). With enhancements to the spatial resolution, it gained usage in civil structural applications. Brillouin scattering pertains to the interaction of light in optical fibers with time dependent optical density variations that result in changes to its energy (frequency) and path. The optical density variations may be due to strain or temperature gradients. The Brillouin optical time-domain analysis (BOTDA) method employs the stimulated scattering technique by using both a pulse and a continuous signal (Horiguchi *et al.* 1995; Horiguchi and Tateda 1989; Hotate and Tanaka 2001). The Pulse-Prepump Brillouin Optical Time Domain Analysis (PPP-BOTDA) method is a newer version of BOTDA with a stepped pulse shape. PPP-BOTDA is capable of making dynamic measurements (100 Hz over 1 kilometer) with spatial resolutions as low as 20 cm in the dynamic mode (Kishida et al. 2006). Irrespective of the interrogation approach, the Brillouin frequency shift is linearly dependent on both the temperature and strain in a fiber. The relationships between the Brillouin frequency shift, strain and temperature are given as:

$$v_B(T_r, \varepsilon) = C_S(\varepsilon - \varepsilon_r) + v_{Br}(T_r, \varepsilon_r) \tag{1}$$

$$v_B(T, \varepsilon_r) = C_T(T - T_r) + v_{Br}(T_r, \varepsilon_r) \tag{2}$$

Where, v_B is the Brillouin frequency shift, C_S and C_T are the strain and temperature coefficients, respectively; T_r and ε_r are the strain and temperature corresponding to a reference Brillouin frequency, v_{Br}. Brillouin-based sensing approaches utilize the entire length of the optical fiber for both signal transmission and sensing purposes, and then a

11

distributed sensing with large monitoring range is realized. For strain sensing an auxiliary fiber is employed for temperature compensation.

2.1.2. Analytical Methodology

In establishing the method, formulations involve relating the effect of individual cable forces on the bending moment along the span length of the bridge. Bridge displacements are used in order to account for the interrelationships between all the cables in the bridge when cable tensions are changed in one or more cables. Deck and pylon displacements are also employed as constraints in the formulation of the linear least square procedure for detection and quantification of the forces in the affected cables. The cable-stayed bridge shown in Figure 1 is employed for deriving the basic equations between the cable forces and the deck strain. In doing so the bridge is represented as a simply supported bridge by removing the middle support and replacing it with a force equal to the support reaction. The cables are also removed and replaced by concentrated forces representing the vertical components of cable forces. The effect of horizontal components of cable forces on flexural strain of the deck is assumed to be negligible. The cable tensions and the concentrated forces on the simple supported bridge are related by:

$$F_i = \frac{P_i}{Sin(\theta_i)} \tag{3}$$
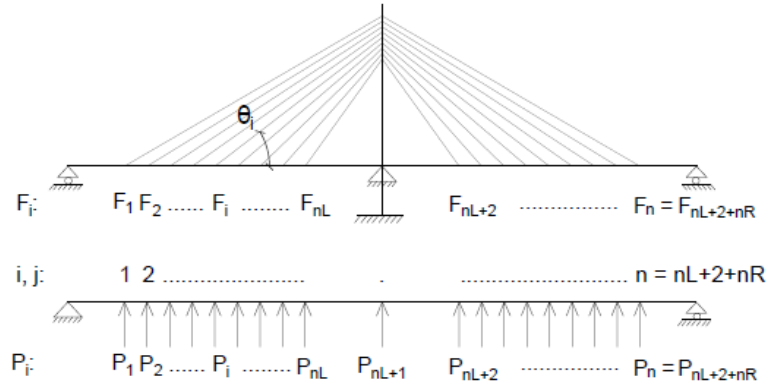
Figure 1. Idealization of the cable-stayed bridge by a simply supported bridge

Where, F_i is tension in cable i; P_i at locations i represent the concentrated forces on the bridge, i.e. interior support reactions and the vertical components of the cable forces, θ_i is the inclination angle of cable i with respect to the deck. For the support reactions, θ_i is $\frac{\pi}{2}$.

The bending moments at individual sections of the bridge in Figure 1 are given by:

$$M_i = \sum_{j=1}^{n} P_j M_{ij} \tag{4}$$

Where, M_i is the bending moment at location i, M_{ij} is the bending moment at location i due to a unit vertical force at point j and n is the total number of cables and the interior supports. By expanding Equation (4) to points along the length of the bridge, a system of equations can be developed relating the bending moment distribution along the entire length of the bridge to the cable forces:

$$C \cdot X = G \tag{5}$$

Where,

$$C = \begin{bmatrix} M_{11} & \cdots & M_{1n} \\ \vdots & \ddots & \vdots \\ M_{n1} & \cdots & M_{nn} \end{bmatrix} \tag{6}$$

$$X = \begin{bmatrix} P_1 \\ \vdots \\ P_n \end{bmatrix} \tag{7}$$

$$G = \begin{bmatrix} M_1 \\ \vdots \\ M_n \end{bmatrix} \tag{8}$$

The vector G pertains to the distribution of bending moment along the length of the deck, and it is experimentally measured, i.e. from the distributed measurement of flexural strains by BOTDA. The relationship between the bending moment M_i and the flexural strain is obtained from the flexure formula:

$$M_i = \frac{\epsilon_i EI}{C} \tag{9}$$

Where I is the moment of inertia of the bridge cross-section, C is the distance from the neutral axis to the location of the strain sensor, generally the outermost cross-section fiber, E is the modulus of elasticity of the section, and ϵ_i is the strain at location, i. EI is the bending stiffness of the bridge deck. M_{ij} are computed through sequential placement of unit forces along the span length. Assuming the dead load remains constant prior and after the damage, the bending moment is independent of the dead loads once the undamaged

state of the deck is subtracted from the damaged state. It is then possible to determine the cable forces and support reactions (force vector *X*) from the solution of Equation (5).

BOTDA provides distributed measurement of strain, but in Equation (5), the bending moment terms, M_i are discretized. Discretization of distributed strains is accomplished considering that the Brillouin sensors provide weighted average of strains within the spatial resolution of the system along the sensor length. The averaged strain obtained by BOTDA at any section, *i*, along the sensor length can be written as (Yamauchi et al. 2007):

$$\bar{\epsilon}_i = \frac{1}{\int_{-\frac{d}{2}}^{\frac{d}{2}} w(s)ds} \int_{-\frac{d}{2}}^{\frac{d}{2}} w(s)\epsilon_i(s)ds \tag{10}$$

Where, *d* is the spatial resolution or the length over which the BOTDA system averages the strain, *s* is the spatial distance along the fiber, $\epsilon_i(s)$ is the true strain at a distance, *s*, from the section under consideration, *i*, and, w, is the weighting function which depends on the shape of the pump pulse (and pre-pump pulse when PPP-BOTDA is used). Considering a rectangular pump pulse, Equation (10) can be simplified as a moving average over the averaging length (Kishida et al. 2005) as follows:

$$\bar{\epsilon}_i = \frac{1}{d}\int_{-\frac{d}{2}}^{\frac{d}{2}} \epsilon_i(s)ds \tag{11}$$

Re-writing Equation (11) in summation form, yields:

$$\bar{\epsilon}_i = \frac{1}{d} \sum_{s=-\frac{d}{2}}^{\frac{d}{2}} \epsilon_i(s)\delta_s \tag{12}$$

Where, δ_s is the increment between measured strain locations, and by using Equation (9)

it will be possible to substitute M_i for ϵ_i in Equation (12), and therefore, $\overline{M_\iota}$ becomes

$$\overline{M_\iota} = \frac{1}{d} \sum_{s=-\frac{d}{2}}^{\frac{d}{2}} M_i(s)\delta_s \tag{13}$$

Substituting Equation (4) into Equation (13) results in

$$\overline{M_\iota} = \frac{1}{d} \sum_{s=-\frac{d}{2}}^{\frac{d}{2}} \sum_{j=1}^{n} P_j M_{ij}^s \, \delta_s \tag{14}$$

Rearranging Equation (14) results in

$$\overline{M_\iota} = \sum_{j=1}^{n} P_j \frac{1}{d} \sum_{s=-\frac{d}{2}}^{\frac{d}{2}} M_{ij}^s \, \delta_s \tag{15}$$

$$\overline{M_\iota} = \sum_{j=1}^{n} P_j \, \overline{M_{\iota J}} \tag{16}$$

Where M_{ij}^s is the bending moment at a distance s from section i due to a unit vertical force

at section j. Equation (5) can be re-written in expanded form to account for all the locations

along the length of the bridge, but this time in terms of discretized bending moment distribution (averaged within spatial resolution) along the entire length of the bridge to the cable forces:

$$\bar{C}.X = \bar{G} \tag{17}$$

Where,

$$\bar{G} = \begin{bmatrix} \overline{M_1} \\ \vdots \\ \overline{M_n} \end{bmatrix} \tag{18}$$

$$\bar{C} = \begin{bmatrix} \overline{M_{11}} & \cdots & \overline{M_{1n}} \\ \vdots & \ddots & \vdots \\ \overline{M_{n1}} & \cdots & \overline{M_{nn}} \end{bmatrix} \tag{19}$$

In practical applications, the inherent noise associated with the distributed measurements with Brillouin based systems needs to be considered in Equation (17). Depending on the spatial resolution selections in the measurement system, the noise levels range between seven to fifteen percent of the total output. At these levels only larger changes in the cable forces could be discerned, and the system would fail to recognize the force changes in the adjoining cables. A mere signal smoothing algorithm may not be sufficient to preserve the signal details, especially as it involves the interrelationship between the cable forces and structural displacements. To account for this, Equation (17) is subjected to bridge displacement constraints and solved as a constrained linear least-squares problem. Considering that the cables are anchored both to the deck and the pylons, Hegab (1986)

developed the following relationship for computing the forces in the cables:

$$F_i = \frac{E_i A_i}{L_i}(-Y_i \sin\theta_i \pm \Delta_i \cos\theta_i) \tag{20}$$

Where E_i, A_i and L_i are the young's modulus, cross-sectional area and length of the cable i, respectively. Y_i is the vertical deflection of the deck at point i and Δ_i is the pylon horizontal displacement at the connection of cable i with the pylon that is connected to. The negative sign in conjunction with the deck deflection term, Y_i signifies that the downward Y direction is negative. Moreover, for the pylon displacements, displacements away from the cables under consideration are considered positive. The interrelationship between the bridge displacements and the cables is shown in Figure 2.
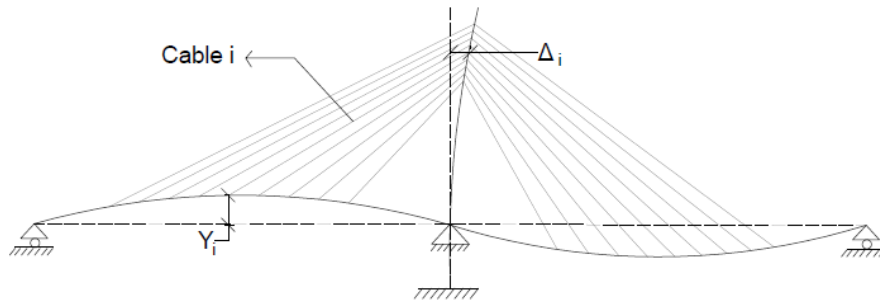
Figure 2. Interrelationship between cables, pylon, and deck displacements

The computational approach employs the imposed constraints in a trial and error procedure in order to compute the change in cable forces. As discussed earlier, the Brillouin based

measurements provide the change in distributed strains based on reference measurements.

The trial and error procedure begins by assuming various levels of tension losses in

individual cables subjected to the imposed displacement constraints, and selects the cable

that has minimized the error associated with the system noise. By substituting Equation

(1) into Equation (20), the interrelationship between the cable forces and bridge

displacements can be written in the following form:

$$\frac{P_i}{Sin(\theta_i)} = \frac{E_i A_i}{L_i}(-Y_i \sin\theta_i \pm \Delta_i \cos\theta_i) \tag{21}$$

The relationship between deck displacements and the cable forces can be stated in terms of

flexibility coefficients:

$$Y_i = \sum_{j=1}^{n} P_j f_{ij}^b \tag{22}$$

Where, f_{ij}^b is deflection of the deck at section i due to a unit force at section j. Similarly,

the flexibility of the pylon can be stated as:

$$\Delta_i = \sum_{j=1}^{nL}(Q_j - Q_{nL+2-j})f_{ij}^p \tag{23}$$

Where $Q_j = P_j \cot\theta_j$ is the horizontal component of tension in cable j; f_{ij}^p is the

displacement of the pylon, p, at the location of cable number i on the pylon due to a unit

horizontal force at the location of cable j; nL is the number of cables that are connected to

the same side of the pylon with respect to cable j, and $nL + 2 - j$ is the cable that is

connected at the location of cable j but on the opposing face of the pylon. Eqs. (22) and

(23) are used for substituting for Y_i and Δ_i into Equation (21). After rearranging the terms,

the constraint relating the cable forces to the deck and pylon displacements for any cable t

located on the left side of the pylon shown in Figure 1 can be written as:

$$
-\frac{L_t}{E_t A_t \sin(t)} P_t + \sum_{j=1}^{nL} \left(-\sin\theta_t f_{tj}^b - \cos\theta_t \cot\theta_j f_{tj}^p \right) P_j
$$

$$
- \sin\theta_t f_{t,nL+1}^b P_{nL+1} \tag{24}
$$

$$
+ \sum_{j=nL+2}^{nL+1+nR} \left(-\sin\theta_t f_{tj}^b + \cos\theta_t \cot\theta_j f_{tj}^p \right) P_j = 0
$$

Where, nL and nR are the number of cables on the left and right sides of the pylon,

respectively. Similarly, the following relationship is obtained for any cable t on the right

side of the pylon:

$$
-\frac{L_t}{E_t A_t \sin(t)} P_t + \sum_{j=1}^{nL} \left(-\sin\theta_t f_{tj}^b + \cos\theta_t \cot\theta_j f_{tj}^p \right) P_j
$$

$$
- \sin\theta_t f_{t,nL+1}^b P_{nL+1} \tag{25}
$$

$$
+ \sum_{j=nL+2}^{nL+1+nR} \left(-\sin\theta_t f_{tj}^b - \cos\theta_t \cot\theta_j f_{tj}^p \right) P_j = 0
$$

Eqs. (24) and (25) are written for each intact cable t of the bridge under consideration. Considering the boundary conditions, i.e. zero deflections at bridge supports, the boundary condition constraint can be written as:

$$\sum_{j=1}^{n} P_j f^b_{nL+1,j} = 0 \qquad (26)$$

Therefore, sufficient numbers of constraints can be established to match the number of unknown intact cable forces and interior support reactions. Equation (17) can now be solved subjected to the aforementioned constraints with the assumed trial and error values for the location and magnitudes of tension force losses. The trial and error procedure is repeated until the assumed cable force returns the minimum norm residual of the least-square solution, which yields the location and the amount of tension that the damaged cable has actually lost. Mathematically, different assumptions for the cable k and P_k are made to minimize Equation (27) and the assumption that minimizes R in Equation (27) is the solution.

$$R = \|C \cdot X - G\|_2^2 \qquad (27)$$

Where R is the squared of the Euclidian norm of the vector $C \cdot X - G$, and X is the result of the constrained linear least squares.

In summary, the linear least squares approach determines the loss in cable tension by solving Equation 27 such that the boundry constraints listed in Equations 24, 25 and 26 are

not violated. In the next chapter, the efficiency of this theoretical approach is evaluated through experimentation and finite element analysis.

Even though distributed sensing has considerable advantages in monitoring the entire cable stays using a single line of fiber optic cable, certain projects may benefit from implementation of discrete sensors. Examples include physical and geometrical constraints for the installation of the distributed sensors. Hence, in the next section, a different analytical solution will be introduced to determine the cables tension loss by means of discrete sensors. This approach will also utilize optimization of a linear program.

2.2. Recursive Optimization Approach Using Point-style Sensors

The analytical approach proposed in this section utilizes the change in support reactions to detect damage in cables of single-plane cable stayed bridges. Considering that the cables are anchored both to the deck and the pylons, Hegab (1986) introduced the following equation to obtain the cable forces:

$$F_j = K_j(Y_j\sin\theta_j \pm \Delta_j\cos\theta_j) \tag{28}$$

Where K_j is the stiffness of the cable j. Y_j and Δ_j are the deck vertical displacement and pylon horizontal displacement respectively, at the connection point with the cable j. It is apparent from equation (28) that loss of cable stiffness will result in reduction of the cable

force. Ultimately, the girder deflection and the reaction force at the support will increase. The amount of force transferred to the supports depends on the stiffness of the cables, the girders and the pylons. Hence, when a cable is damaged, a portion of the cable tension loss is transferred to the supports. In essence, changes in the support reactions are effective parameters to localize and quantify the damage in stay cables. Change in support reactions from each adjacent span can be obtained by computing the change in shear forces of deck structural elements. The shear forces from each adjacent span of the support of the truss girder cable-stayed bridges can be obtained using the axial strain in the web members of the support region (Figure 3) using the following equation:

$$V = \varepsilon E A sin\theta \tag{29}$$
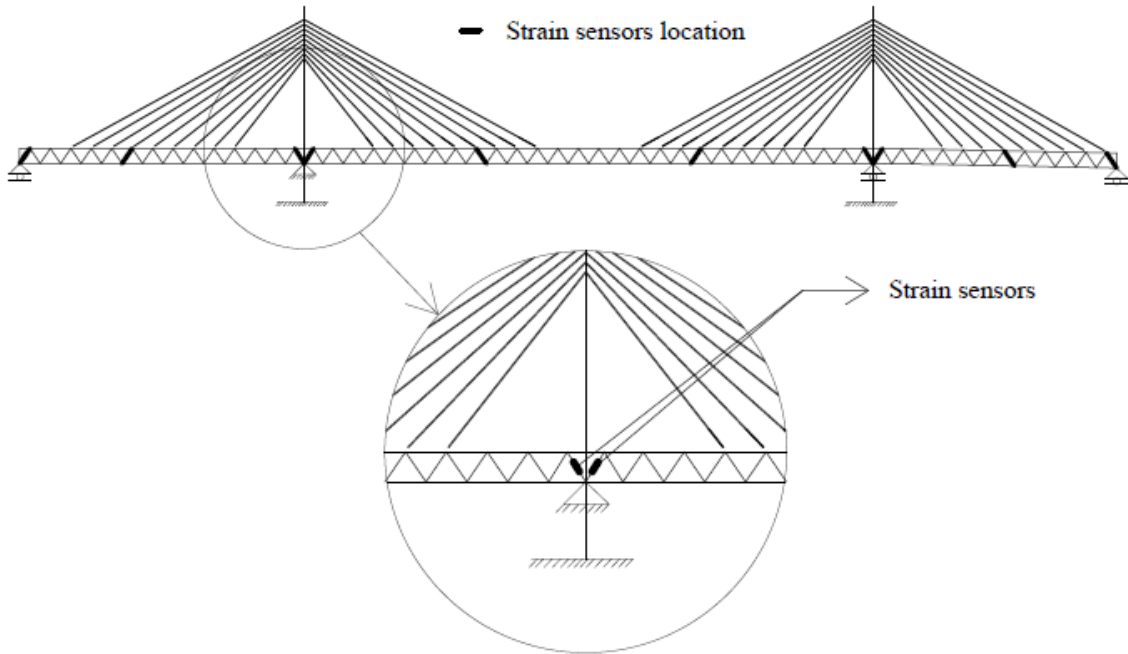
Figure 3. Detection of support reactions from diagonal truss elements strains

Where ε, E, A and θ are the axial strain, modulus of elasticity, cross-sectional area and inclination angle of the truss web member respectively.

The support reactions in box girder bridges can be obtained either by strain rosette sensors (Gere and Timoshenko, 1990; Bao et al., 2015) or by bending strain gauges and the differential relationship between the bending moment and shear, and linearity of the bending strain near the supports. The linearity of the bending moment between the support and the neighboring cable is due to the fact that the difference in strains prior and after the damage are independent of the dead load. By placing strain gauges at the indicated locations in Figure 4, the change in shear force from each adjacent span of the support can be obtained from the bending moment as follows:

$$V_i = \frac{\Delta M_i}{\Delta x_i} \tag{30}$$

Where,

$$\Delta M_i = \Delta \varepsilon_i \left(\frac{EI}{y}\right) \tag{31}$$

Where $i=1...m$, m is the number of adjacent sides of individual supports as shown in Figure 4, Δx is the distance between the bending strain sensors at the support and the neighboring cable (Figure 4), $\Delta \varepsilon$ is the difference between measured strains by the two strain sensors,

24

ΔM_i is the change in bending moment between the locations of two strain sensors, I is the moment of inertia of the bridge cross-section, y is the distance from the neutral axis to the location of the strain sensor, generally the outermost cross-section fiber, and E is the elastic modulus of the section material.
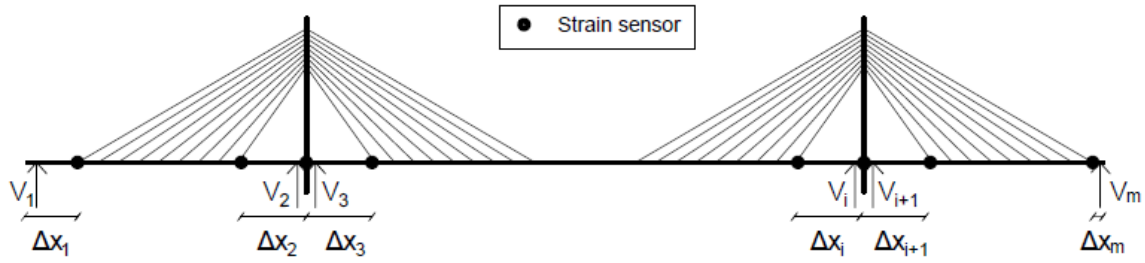
Figure 4. Locations of bending strain sensors and bridge shear forces

The implementation of this method requires employing strain sensors at both sides of the supports in order to determine the change in shear force from adjacent spans. The change in shear forces prior and after the damage can be vectorially written as:

$$V = V^d - V^u \tag{32}$$

Where $V^d = \{V_1^d | V_2^d | \dots | V_m^d\}^T$ and $V^u = \{V_1^u | V_2^u | \dots | V_m^u\}^T$ are the vectors representing the bridge shear forces on adjacent sides of individual supports in damaged and undamaged cables state, respectively. The resulting vector V is dead load independent assuming the dead load remains unchanged prior and after the damage.

The location of damaged cables and their damage intensity, i.e. tension losses, can then be determined by minimizing the Euclidean norm in equation (33):

$$I = \|S \cdot X - V\|_2^2 \tag{33}$$

Where,

$$S = \begin{bmatrix} S_{11} & S_{12} & \cdots & S_{1n} \\ S_{21} & S_{22} & \cdots & S_{2n} \\ \vdots & \vdots & \ddots & \vdots \\ S_{m1} & S_{m2} & \cdots & S_{mn} \end{bmatrix} \tag{34}$$

$$X = \begin{bmatrix} x_1 \\ x_2 \\ \vdots \\ x_n \end{bmatrix} \tag{35}$$

n is the number of cables, X is the vector of cable forces which represents the location and intensity of damaged cables, I is the Euclidean norm and S is the sensitivity matrix, i.e. S_{ij} is the change of the deck shear force at the support face i due to a unit stiffness loss in cable j. S_{ij} can be determined using finite element model analysis and applying a unit stiffness loss in each cable j.

The optimum solution for X in equation (33) can be obtained when:

$$X = (S^T S)^{-1} S^T V \tag{36}$$

The sensitivity matrix needs to be updated when the cable stiffness change. A recursive approach is employed for updating the sensitivity matrix, where at each iteration step, the cable stiffness are updated as follows:

$$K_j^t = \frac{x_j^t}{F_j^0} K_j^0 \tag{37}$$

Where, K_j^0 and F_j^0 are the stiffness and tensile force of cable j in undamaged state, respectively, x_j^t is the calculated loss of tensile force in cable j at iteration step t based on equation (36). Iteration is repeated until the cable force differences between two successive iterations remain below an acceptable tolerance value. Mathematically, the final iteration is achieved when:

$$\left| \frac{x_j^t - x_j^{t-1}}{x_j^t} \right| < \tau \tag{38}$$

Where, x_j^t and x_j^{t-1} are the detected tension loss in cable j for two successive iterations, and τ is the tolerance level.

In practical applications, the inherent noise associated with the measured strains can result in non-physical solution of equation (36). To account for this, the solution of equation (36) is bounded to non-negative results. Negative results are non-physical since they indicate increase in the cable tensile force due to loss of cable stiffness.

In the proposed approach the change in shear force vector: $V = \{V_1|V_2| \dots |V_m\}^T$ is computed by measuring the shear strains. The sensitivity matrix is obtained by assuming: $K_j^1 = K_j^0$, for the initial iteration step $t = 1$. Then, equation (36) is solved for the cable force losses, X^t. Equation (37) is employed for updating the cable stiffness, K_j^t, and the

sensitivity matrix, S is recomputed. The process is recursive and the iteration step is increased each time (i.e. $t = t + 1$) until τ in equation (38) converges to the acceptable level.

In the next chapter, the efficiency of this approach is evaluated through experimentations and finite element analysis for a series of damage scenarios. The experimentations employ strain sensors to determine the shear forces, and then Equation 38 is utilized to determine the loss in cable forces.

The previous two sections pertained to two theoretical approaches for detection of tension loss in the cables of cable stayed bridges. In the next section, a different theoretical approach based on machine learning will be presented to determine damage in the building structures by means of load tests.

2.3. Machine Learning Based Assessment of Damage in Building Structures

Machine Learnings (ML) is a subset of artificial intelligence which is widely used for pattern classification. In particular application to the present application, the structural model is trained with a set of input data, i.e., the change in strain magnitudes under known loading configurations. Once the model has been trained in this fashion, it will be employed to predict the damage for any other loading conditions that the structure was previously never exposed to. Formulation of the method begins by the stiffness equation

of the structural system expressed as:

$$F = KU \tag{39}$$

Where, F is the load matrix, K is the stiffness matrix, and U is the displacement matrix, which is related to the strain in the structural members. By placing strain sensors in the selected sections of a structure and imposing known loads, F, the change in strain due to the loads can be written as (Figure 5):

$$V = V^d - V^u \tag{40}$$

Where, $V^d = \left\{ \varepsilon_{1,d}^i \middle| \varepsilon_{2,d}^i \middle| \dots \middle| \varepsilon_{m,d}^i \right\}^T$ and $V^u = \left\{ \varepsilon_{1,u}^i \middle| \varepsilon_{2,u}^i \middle| \dots \middle| \varepsilon_{m,u}^i \right\}^T$ are strain vectors for damaged and undamaged states, respectively. $\varepsilon_{t,d}^i$ and $\varepsilon_{t,u}^i$ are the strains at location t due to the load F_i in damaged and undamaged states, respectively. The strain vector V is the difference between the strain magnitudes of undamaged and damaged states. This vector is then used as input to the ML models described herein to interpret the output, which in this case pertains to structural damage.
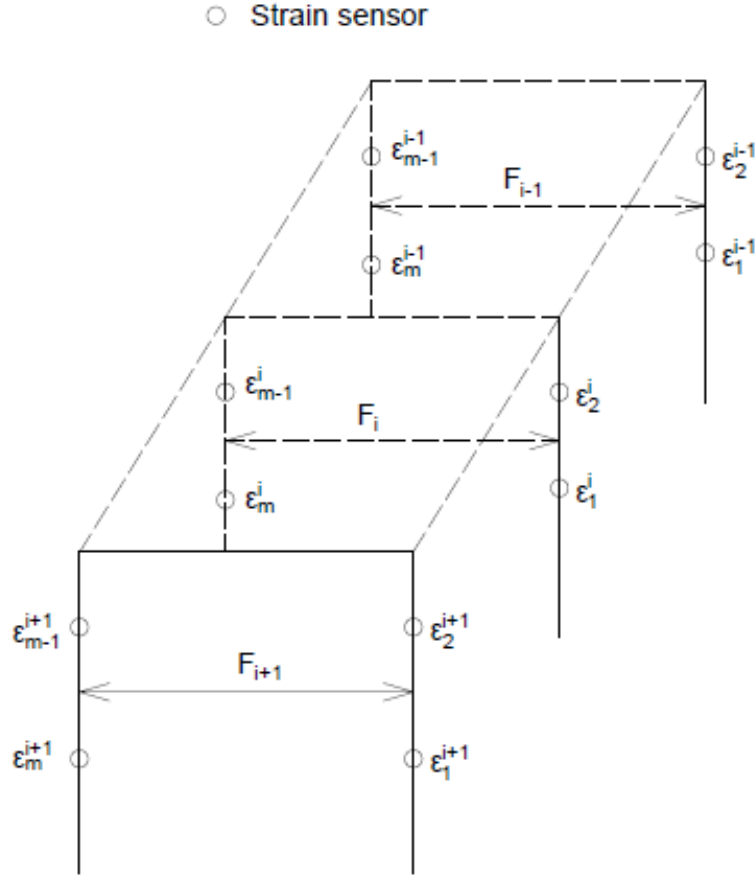
Figure 5. Load and sensor configurations in a series of frame members

2.3.1. Training

Training of the model is accomplished by simulating a series of possible damage cases using finite element analysis. The strain vector, V, is extracted from the finite element model for every possible damaged case. The strain vector is used as input, and the damaged scenario is used as output to train the model. Once the ML model is trained for all possible

damage scenarios, the model will then be capable of predicting the damage for a given strain vector. There exists a number of machine learning methods. In this thesis, the performance of NN, SVM and GNB are evaluated and compared for damage detection.

2.3.2. Neural Networks

Neural Networks (NN) were inspired by how the human brain works and they act as a mathematical tool in predictive modeling (Hippert et al, 2001). Neural networks consist of an arbitrary number of layers. One of the most popular networks is multi-layer feed-forward network. This network consists of input layer, hidden layer(s) and output layer. In this study, the input layer pertains to the strain vector, V, as determined in section 2. The output layer pertains to the damage case number. The architecture of the applied feed-forward network which was utilized in this thesis is depicted in Figure 6.
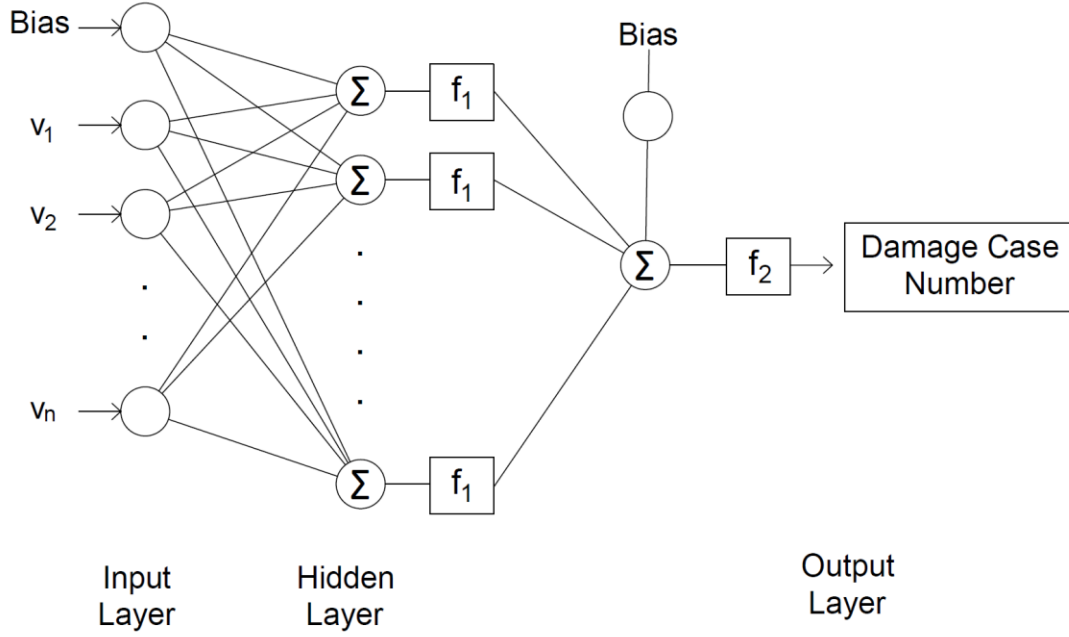
Figure 6. Feed-Forward neural network architecture

Where $V = (v_1, v_2, .. v_n)$ is the strain vector, as explained in section 2, f_1 is the hyperbolic tangent function and f_2 is a linear activation function. In this study, 100 nodes were used in the hidden layer. The model is first trained by sending the strain vector, V, as the input to the network for various damage cases. The relationship between the layers is then determined by Backpropagation algorithm (Hagan et al, 1994) to achieve the correct damage case number for a given training input.

2.3.3. Support Vector Machine

SVMs are a relatively new supervised learning approach that are capable of handling noisy data. They have been used in a number of applications from cancer diagnosis (Furey et al, 2000) to text classification (Tong et al, 2001). In simple words, SVMs are hyper planes that are chosen such that the strain vectors are separated with a maximal margin. Margin is defined as the distance between the closest strain vectors to the hyper plane. In simple terms, the hyper plane will separate the strain vectors with hyper planes, such that two sides of the hyper plane represent two different damage case scenarios.
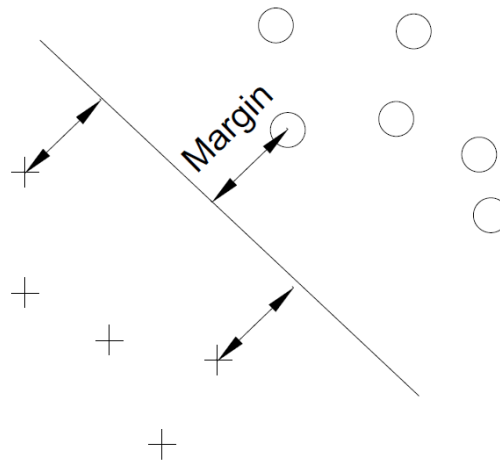
Figure 7. SVM classifier and margin

One can prove that the hyper plane decision boundary for strain vector, *V*, can be written

as (Furey et al, 2000)

$$f(V) = sign(W^T \varphi(V) + b)$$
(41)

Where *sign* is the signum function, b is the bias term, $\varphi(.)$ is a mapping function. Mapping function allows separation of non-linear strain vectors by mapping the strain vector to a higher dimensional space. In this study, radial basis kernel function was employed to map the strain vector to a higher dimensional space. W is the weights vector. It has been proven that the maximal margin hyper plane between the strain vectors is obtained when (Furey et al, 2000):

$$W = \sum_{i=1}^{n} \alpha_i \, y_i \varphi(V_i)$$
(42)

where *n* is the number of the possible damage cases used in training, y is the binary output which defines the damage case that a strain vector belongs to, and α_is are positive coefficients that maximize the following equation

$$\sum_{i=1}^{n} \alpha_i - \sum_{i,j}^{n} \alpha_i \alpha_j \, y_i y_j \varphi(V_i)^T \varphi(V_j)$$
(43)

such that

$$\sum_{i=1}^{n} \alpha_i y_i = 0$$
(44)

Hence, one can determine the alpha coefficients by solving Equation 5 using the method

of Lagrange multipliers. In this study, we have more than two damage cases. Hence, a one-versus-one approach (Milgram et al., 2006) was implemented in order to classify all possible damage cases.

2.3.4. Gaussian Naïve Bayes

Gaussian Naïve Bayes (NB) is a statistical approach based on probabilities and Bayes theorem (John and Langley, 1995). GNB assumes that the predictors, that are considered to be the sensors data in this thesis, are independent from each other. GNB estimates the probability for all possible damage cases. The damage case that has the highest probability is then considered to be the predicted damage case. Using the Bayes theorem, the conditional probability of the damage case d_i for a given set of sensors data can be written as (John and Langley, 1995)

$$P(d_i|V) = \frac{P(V|d_i)P(d_i)}{P(V)} \qquad (45)$$

Where $V = (v_1, v_2, .., v_n)$ is the strain vector and $P(.)$ is the probability function. Since the output of sensors are independent from each other, one can write

$$P(V|d_i) = \prod_t P(v_t|d_i) \qquad (46)$$

where $P(v_t|d_i)$ is normally distributed. The predicted damage case, d, is then obtained by

35

$$d = argmax_i \, P(d_i|V) \tag{47}$$

Where argmax is arguments of the maxima. In this expression, arguments of maxima pertains to the damage case i that maximizes the function $P(d_i|V)$.

The efficiency of the three machine learning approaches described in this section is evaluated through field implementations in chapter 4.

In summary, in this chapter three different theoretical approaches were proposed for structural health monitoring of buildings and cable-stayed structures. Discussion of the performance, limitations and advantages of these techniques is an important considertation for any structural health monitoring method. Hence, the next two chapters pertain to evaluation of these three theoretical approaches through experimentations and field implementations.

CHAPTER 3

3. EXPERIMENTAL VERIFICATION

The content of this chapter was published as "Nazarian E, Ansari F, Zhang X, Taylor T (2016) Detection of Tension Loss in Cables of Cable-Stayed Bridges by Distributed Monitoring of Bridge Deck Strains. Journal of Structural Engineering, 142(6), 04016018" and "Nazarian E, Ansari F, Azari H (2015). Recursive optimization method for monitoring of tension loss in cables of cable-stayed bridges. Journal of Intelligent Material Systems and Structures, 1045389X15620043". Reproduced with permission from ASCE and Journal of Intelligent Material Systems and Structures.

The theoretical damage assessment methodologies for the cable stayed bridge developed in the earlier chapter of this thesis are evaluated in this chapter. The two approaches are examined using both numerical simulations and laboratory experiments. The structure under study is a $\frac{1}{60}$ reduced-scale cable-stayed bridge. In evaluating the efficiency of the proposed methods, various different damage case scenarios were examined on this scaled model to ensure the robustness of the methodology.
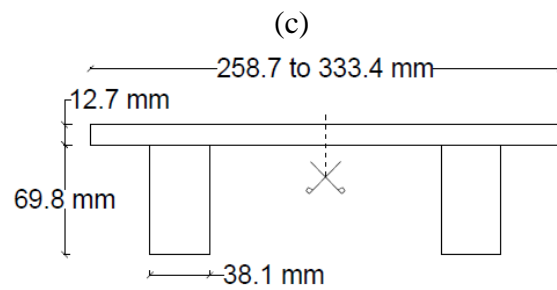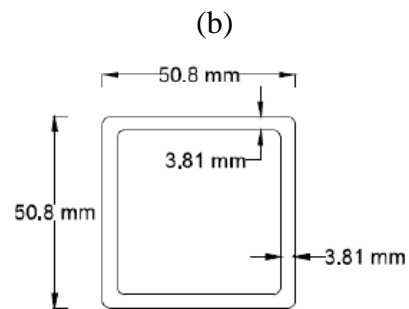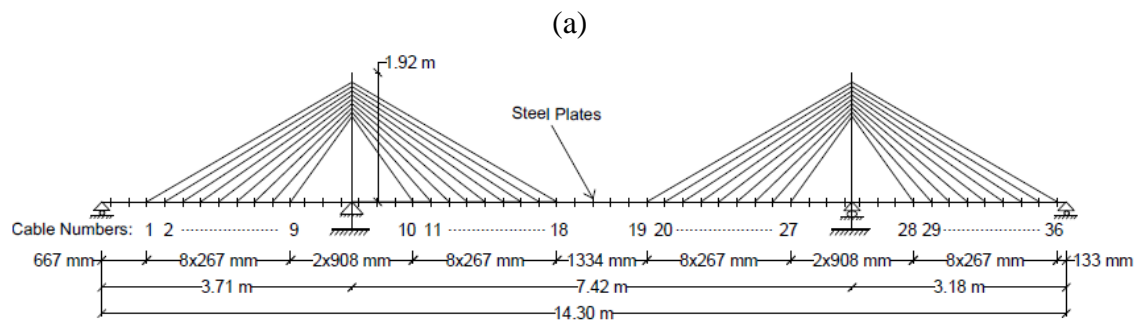
3.1. Experimental Program

The experimental program was designed to evaluate the efficiency of the proposed method for monitoring the cable forces by distributed measurement of strain along the span lengths of the bridge. The approach taken here was to examine the applicability of the method through development of a realistic experiment. Therefore, a reduced scale model of an

actual bridge, Chongqing Dongshuimen Yangtze River Bridge, which was designed and built by earlier researchers in the Smart Sensors and NDT laboratory was employed for this purpose. The main bridge is a double tower single cable plane, cable-stayed steel truss Girder Bridge, with three spans of 222.5, 445, and 190.5 meters, respectively. This bridge was selected because the method was developed for a single plane cable-stayed bridge, and the owners provided access to the bridge plans during the construction of the bridge in cooperation on an international program (NSF-PIRE). The bridge opened to traffic in late March 2014.

The scaled dimensions of the model is schematically depicted in Figure 8a, and the photo of the bridge in the laboratory along with the BOTDA strain measurement system is shown in Figure 8d. A scaling factor of $\frac{1}{60}$ was employed for the model based on the elastic direct method for scaling. In direct modeling, strains and deformations are representative of similar quantities of the prototype structure under the same loading conditions and they are built as a geometric similitude of the prototype (Harris et al. 1999). Detailed discussions regarding the scaling factors are beyond the scope of this article. However, it is important to indicate that the scaling proportions were selected in order to induce the girder strain distributions that are proportional to the real structure under the dead loads and since the prototype cross-section is a boxed truss (Figure 9), a hollow boxed cross-section was selected for the structural model in order to simulate the shape of the prototype cross-section. The deck and the pylons were constructed of steel with yield strength of 235 MPa.

The cross section of the deck is a box with dimensions shown in Figure 8b. Steel piano wires with a diameter of 0.4 mm and tensile strength of 2,500 MPa were employed to represent the stay cables. The pylons were fixed at their bases to the support structure. The moment of inertia for the two pylons were 132,248 mm^4. Additional steel elements were attached to the deck at equal intervals in order to adequately model the dead load of the prototype (Figs. 8 and 10). The cable forces are shown in Table I.

(a)

1.92 m

Steel Plates

Cable Numbers: 1 2 ·············· 9   10 11 ·············· 18   19 20 ·············· 27   28 29 ·············· 36

667 mm   8x267 mm   2x908 mm   8x267 mm   1334 mm   8x267 mm   2x908 mm   8x267 mm   133 mm

3.71 m   7.42 m   3.18 m

14.30 m

(b)

50.8 mm

3.81 mm

50.8 mm

3.81 mm

(c)

258.7 to 333.4 mm

12.7 mm

69.8 mm

38.1 mm
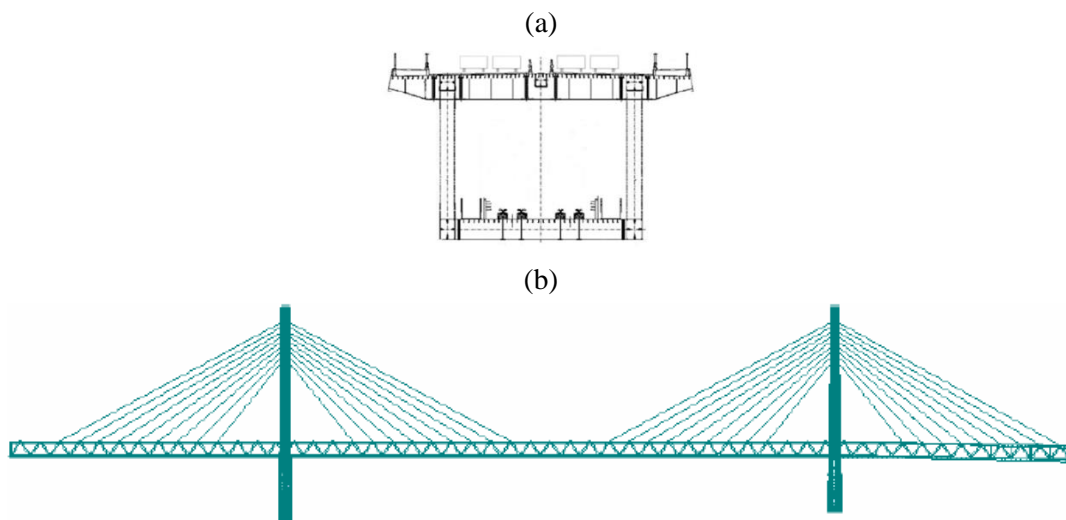
(d)

Figure 8. Structural model

(a) side view; (b) cross-sectional view; (c) steel plates to consider the dead load; (d) schematic view

(a)

(b)

**Figure 9. Prototype bridge: (a) cross-section; (b) side view**

Figure 10. Steel plates and close up view of the adhered distributed fiber

Table I. Cable tensions in intact condition

Cable number	Tension (N)	Cable number	Tension (N)	Cable number	Tension (N)
1	150.8	13	156.1	25	148.6
2	152.6	14	155.2	26	145.5
3	159.7	15	156.1	27	138.8
4	159.7	16	150.8	28	164.1
5	164.6	17	150.3	29	161.0
6	162.8	18	145.0	30	164.1
7	161.5	19	159.2	31	163.7
8	151.2	20	161.5	32	162.8
9	155.2	21	157.0	33	157.0
10	161.9	22	158.8	34	155.7
11	161.5	23	154.8	35	153.9
12	157.9	24	151.7	36	152.6

A telecommunication grade optical fiber (Corning's SMF-28) was employed as strain sensor for monitoring the distributed strain along the length of the bridge deck. A loose fiber was spliced to the strain sensor for measurement and separation of distributed temperatures from the back-scattered Brillouin signals. The distributed sensor was adhered and protected along the entire 14.3-meter length of the deck girder with a silicon-based epoxy. Figure 10 corresponds to the close up view of the adhered sensor on the surface of the bridge deck. A series of strain gauges were adhered to several locations along the deck as independent measures of strains and for comparison with the distributed measurements. The 350 ohms resistance type strain gauges with a range of three percent or 30,000 micro strains were employed for this purpose. Support reactions at the pylons (interior) and edge (exterior) supports were measured by using load cells. The maximum load capacity for the load cells employed at the interior and exterior supports were 68, and 23kgf, respectively. All the load cells were of Wheatstone bridge type with output resistance gauges of 350 ohms, repeatability of 0.05% and hysteresis of 0.15%. The location of strain gauges and the load cells are shown in Figure 11. FBG sensors were adhered to the piano wire cables in order to independently measure the cable forces. The FBGs comprised of Polyimide coated SMF-28 fibers with a maximum strain capacity of 10,000 micro strains. The piano wires with FBGs were calibrated independently after installation on the model against load by successive loading of the wires by external weights. This allowed for transduction of the cable forces during the experiments from the measured FBG strains. A typical

43

calibration response of instrumented piano wire is shown in Figure 12.
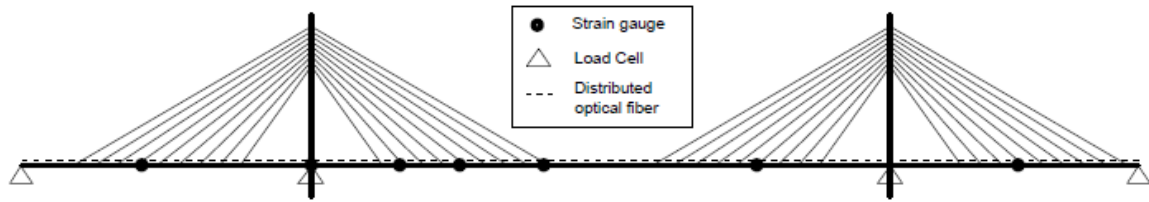
Figure 11. Location of sensors along the bridge span
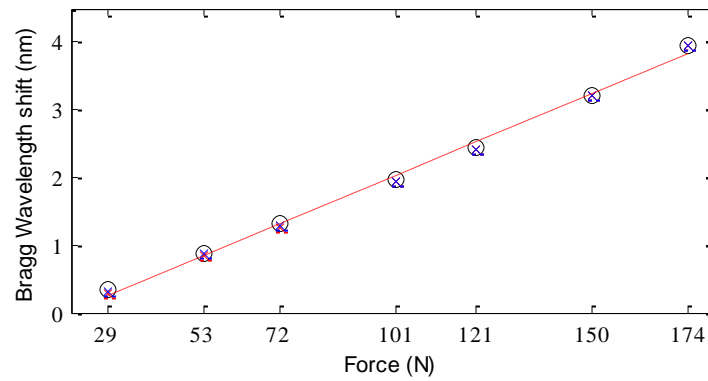
Figure 12. Typical force calibration results for FBG sensor

3.2. Distributed Monitoring of Cable-stayed bridges

3.2.1. Experimental Plan

The experiments included a series of tests in order to evaluate the capability of the method for detection of location as well as the resolution of measurements. Several different

damage scenarios were considered in the experiments as shown in Table II. For instance, experiment numbers 1 through 10 corresponded to single cable damage scenarios at different spans, and cable tension loss levels. Test numbers 11 through 18 pertain to experiments in which two cables incurred tension losses where the affected cables were within various proximities from each other. Experiments 19 and 20 involved cable tension losses in three cables. The experimental program also involved tension losses at levels below thirty percent of the original. However, the resolution of measurements was not sufficient to detect their locations and damage levels with the proposed technique. Therefore, those experiments are not reported here.

Distributed strain measurements were obtained at a spatial resolution of *20 cm*, sampling rate of *1cm* and averaging frequency of 10^{15} with an accuracy of 7 $\mu\epsilon$/0.3°C. The sampling rate of *1 cm* and spatial resolution of *20 cm* were chosen, since the distance between every two cables was about *266 mm*. Decreasing the spatial resolution would have increased the noise level and increasing the spatial resolution to *50 cm*, which is the next possible increment would have led to excessive averaging of the local strain changes.

3.2.2. Results and Discussions

Testing of the model bridge involved straining of the bridge deck by reducing the tensile forces in the bridge cables according to the experimental program outlined in Table II. Turn buckles at the cable anchors were employed for reducing the tension in the cables.

Once the cable forces were reduced to the intended levels, BOTDA was employed for measuring the distributed deck strains. Strain gauges were also employed for measurement of deck strains at selected locations. FBG sensors monitored the cable forces, and load cells measured the support reactions. Data from strain gauges, load cells and FBG sensors provided independent measures for the evaluation of the proposed approach.

Table II. Damage Cases

Damage Case Number	Damaged Cable Number(s)	Percentage of Tension Loss	Damage Case Number	Damaged Cable Number(s)	Percentage of Tension Loss
1	4	30%	2	11	30%
3	4	50%	4	11	50%
5	4	100%	6	11	100%
7	18	30%	8	36	30%
9	18	100%	10	36	100%
11	12	30%	12	12	100%
	23	30%		23	100%
13	12	30%	14	12	100%
	18	30%		18	100%
15	11	30%	16	11	100%
	12	30%		12	50%
17	4	30%	18	4	100%
	11	30%		11	100%
19	4	100%	20	11	50%
	12	50%		12	50%
	23	40%		13	50%

In addition to the experiments, behavior of the bridge model was simulated through nonlinear finite element analysis under the cable force loss scenarios given in Table II. The two dimensional nonlinear FEM model was constructed using commercial software SAP2000. The support conditions, materials and structural properties that were used in modeling are identical to the reduced-scale model, which are described in the experimental program section of this chapter. Frame elements were used for modeling the pylons and deck, and the cables were modeled using cable elements. Figure 13 pertains to the finite element model of the bridge.
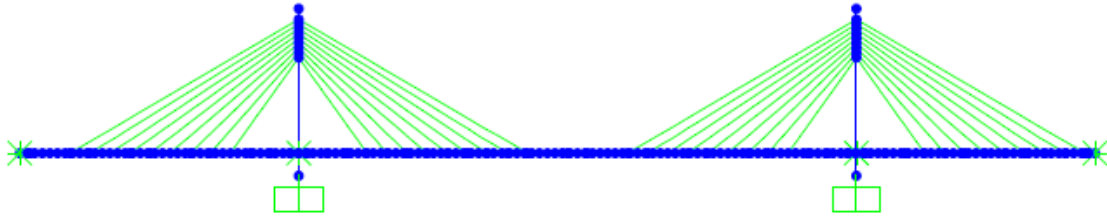
**Figure 13. Finite element model of the bridge**

Raw data acquired from Brillouin systems contain noise that needs to be processed prior to use. A number of signal processing routines have been employed for smoothing the back-scattered Brillouin signals, including direct averaging, least squares, and wavelet transforms (Feng et al. 2014). The Savitzky-Golay filter was employed for smoothing the back-scattered signals in this study. This filter uses convolution in filtering the noise by the method of linear least squares through fitting low degree polynomials to successive sets

of adjacent raw data. Typical experimental and simulation results for single cable force loss scenarios are shown in Figures. 14 through 16. Figures. 14.a, 15.a, and 16.a correspond to the raw and filtered distributed strain data, data from the strain gauges, and the finite element simulations. In Figures 14.b, 15.b, and 16.b the change in cable forces and support reactions computed from the distributed strains are compared with the finite element simulations and measurements by FBG sensors and load cells. In a manner similar to the results shown in Figures 14 through 16, Figures 17 through 20 correspond to the damage scenarios in which force in multiple cables experienced losses.

The experimental program was designed in order to examine the capability of the method in detecting the location of the damaged cables irrespective of their position along the bridge deck or their proximities with respect to each other. As shown in Figures 14, 15, and 16, in the case of single cable with damage, it was possible to detect the location of the damaged cable irrespective of the location of the cable along the bridge span. For quantification of change in cable forces, the method performed well in the case of cables losses that resulted in relatively high change of strain. In some cases, such as the ones shown in Figures 14 and 15, the location of the damaged cable could be directly figured out or approximated from the distributed strains on the deck. In other cases, such as the one shown in Figure 16, it would be impossible to detect the location of the damaged cable without application of the proposed method. As shown in Figures 15b, and 16b, the errors in quantifying the change in tension in compare to the nonlinear finite element analysis and

direct measurements by the FBG sensors were 2-6 percent. However, in the case of cables with lower tension losses, i.e. 30 percent in Figure 14b, the error was 50 percent. A number of experiments were performed for tension losses lower than 30 percent (i.e. 10-20 percent loss in cable tension). However, it was not possible to detect the location of the damaged cables with tension losses below 30 percent due to the strain resolution limitations of the BOTDA system. Moreover, in one or two cases, the computational approach resulted in false readings by affecting the neighboring cables. For instance, in the damage scenario shown in Figure 14.b, in addition to cable 4, cables 3 and 5 also exhibited slight losses. As shown in Figure 21, the change in cable force must be sufficiently large in order to strain the bridge deck beyond the 7 micro-strain resolution of the BOTDA.

Similar discussions can be made for the cases with multiple cable damage scenarios. As shown in Figures 17 through 20, the proposed method is capable of detecting the location of all the cables that exhibited tension loss. Specifically, it was possible to detect the location of adjacent cables with 30 to 50 percent of tension loss in each cable as shown in Figures 17b, and 20b for two and three adjacent cables, respectively. Further examination of Figures 14b through 20b also indicate that the computed interior support reactions based on the distributed measurements correlated with the load cell readings and FEM analysis. However, in terms of the quantification of tension losses, the proposed approach did not yield results comparable to the nonlinear FEM analysis.

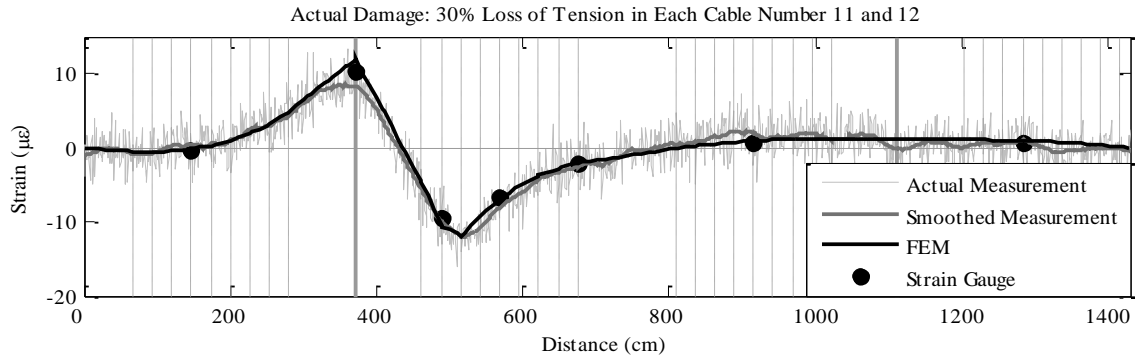Actual Damage: 30% Loss of Tension in Cable Number 4
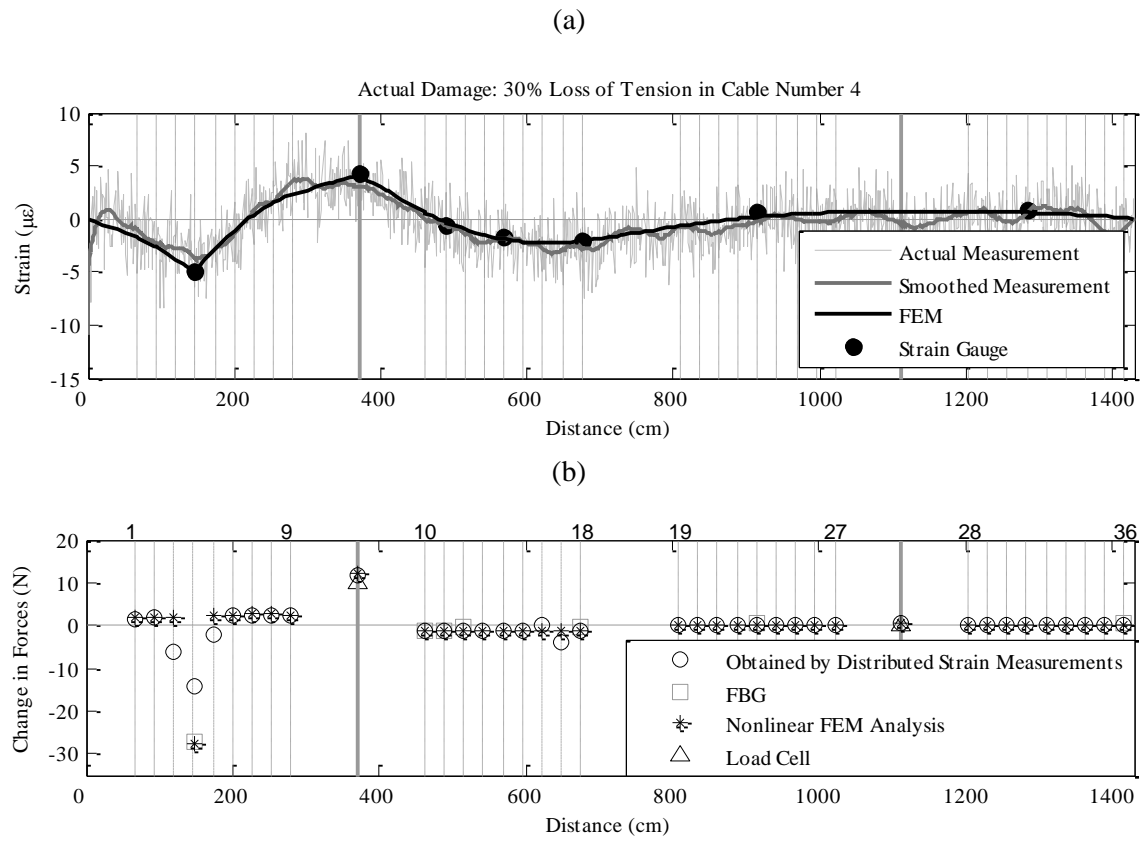
Figure 14. Single cable damage scenario with thirty percent tension loss.

(a)

(b)
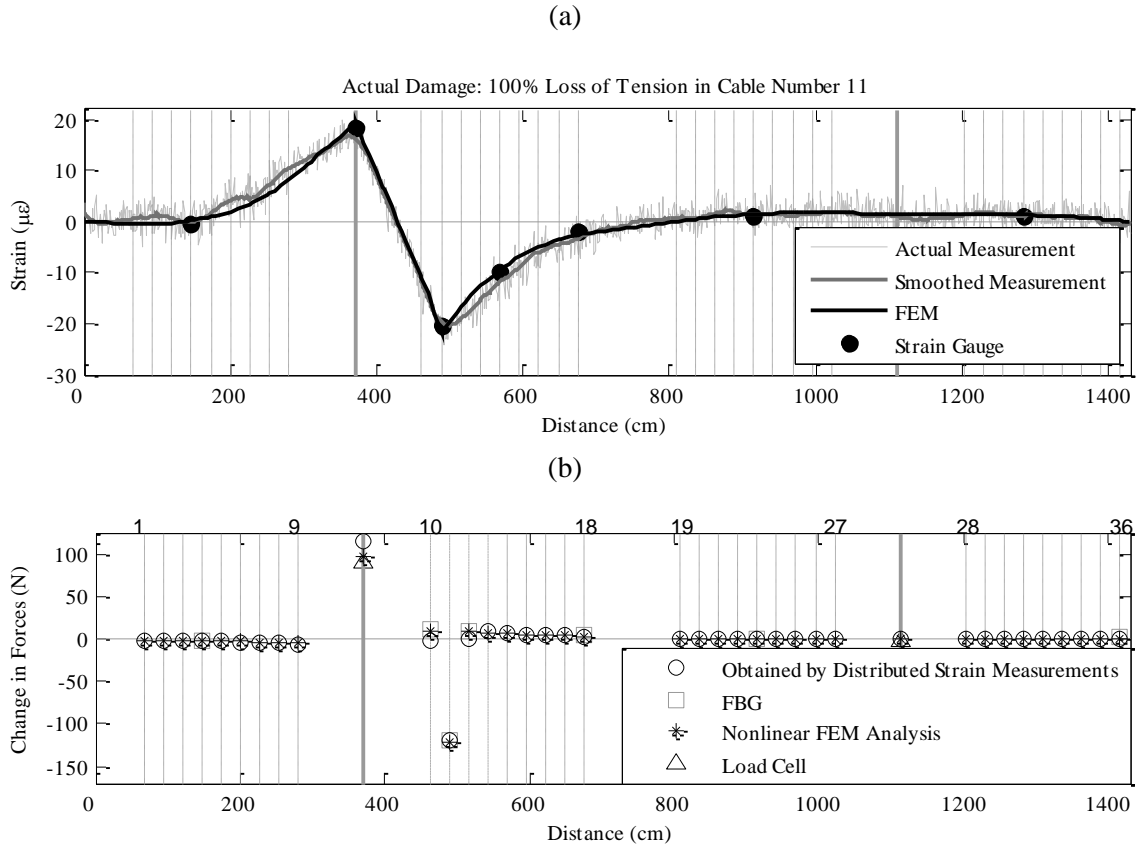
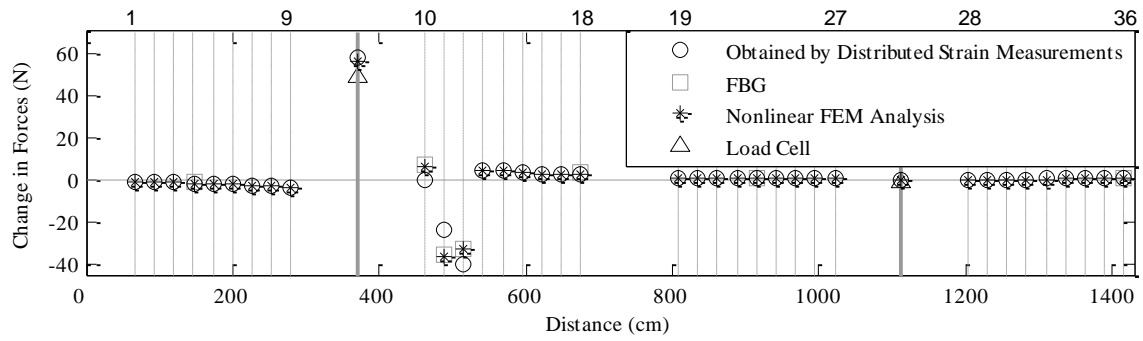**Figure 15. Single cable damage scenario with one hundred percent tension loss**

(a)

Actual Damage: 100% Loss of Tension in Cable Number 36

(b)
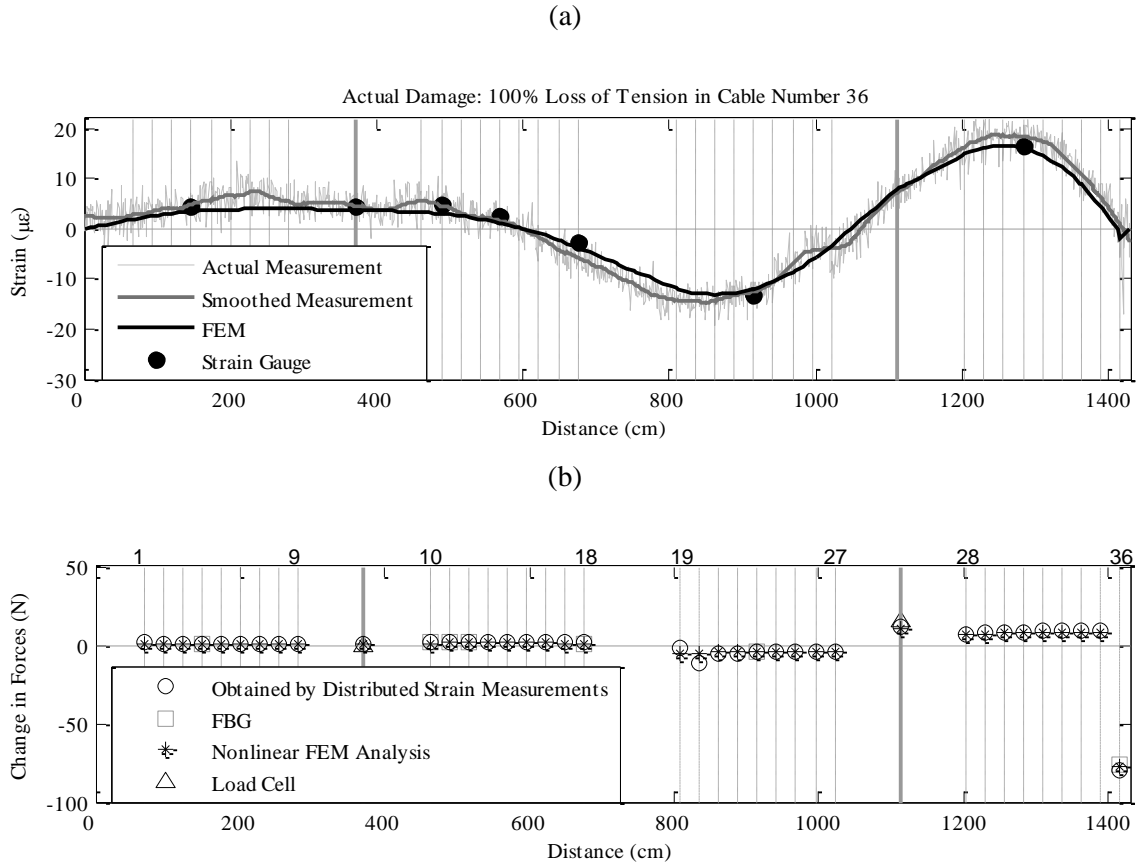
Figure 16. Single cable damage scenario with one hundred percent tension loss

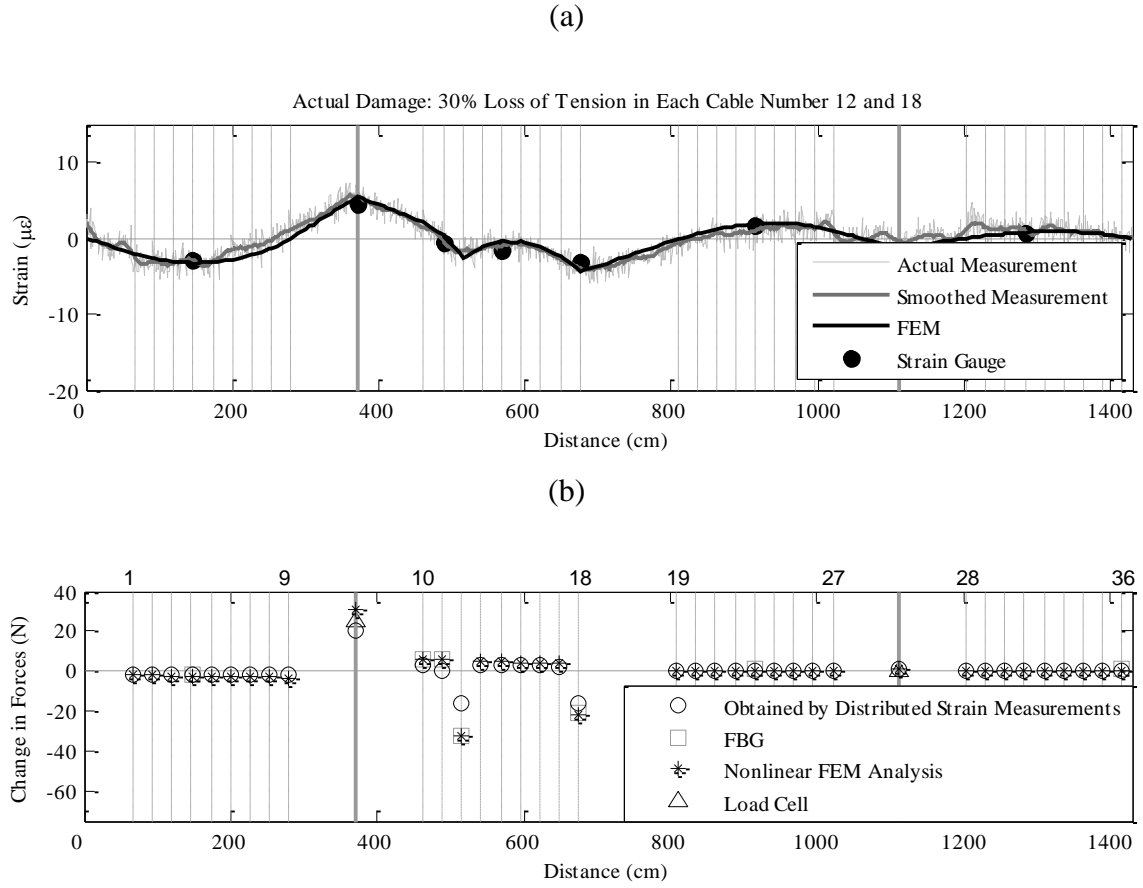Actual Damage: 30% Loss of Tension in Each Cable Number 11 and 12
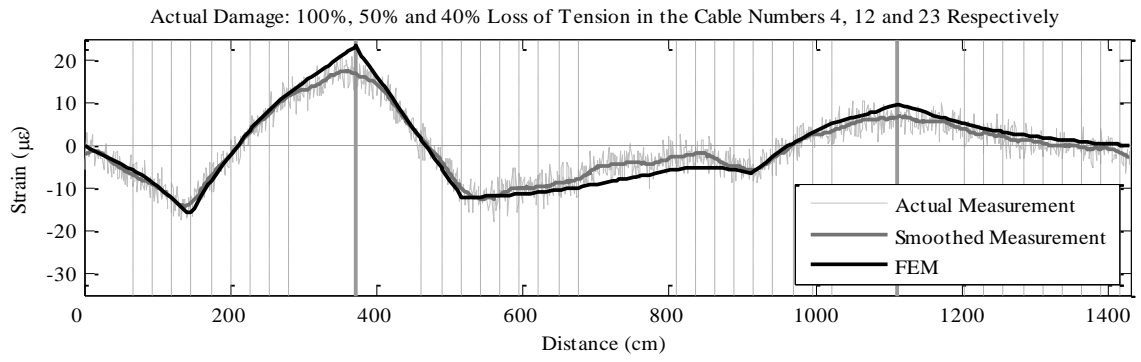
Figure 17. Two-cable damage scenario with thirty percent tension loss in each cable

(a)

(b)

Figure 18. Two-cable damage scenario with thirty percent tension loss in each

(a)

Actual Damage: 100%, 50% and 40% Loss of Tension in the Cable Numbers 4, 12 and 23 Respectively

(b)
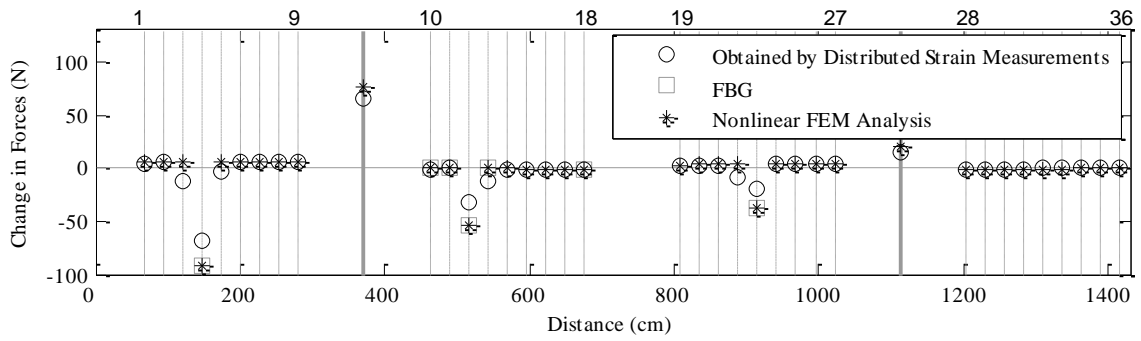
Figure 19. Three-cable damage scenario with various percent tension losses

(a)

Actual Damage: 50% Loss of Tension in Each Cable Number 11, 12 and 13 Respectively

(b)
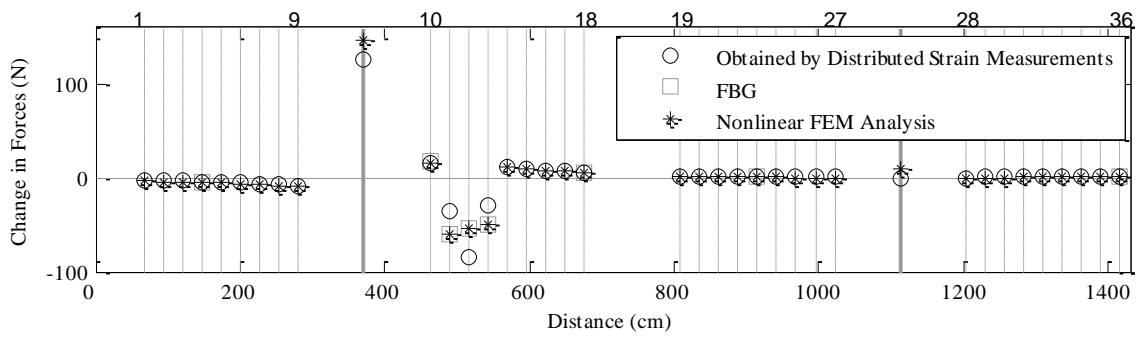
Figure 20. Three-cable damage scenario with fifty percent tension loss

57

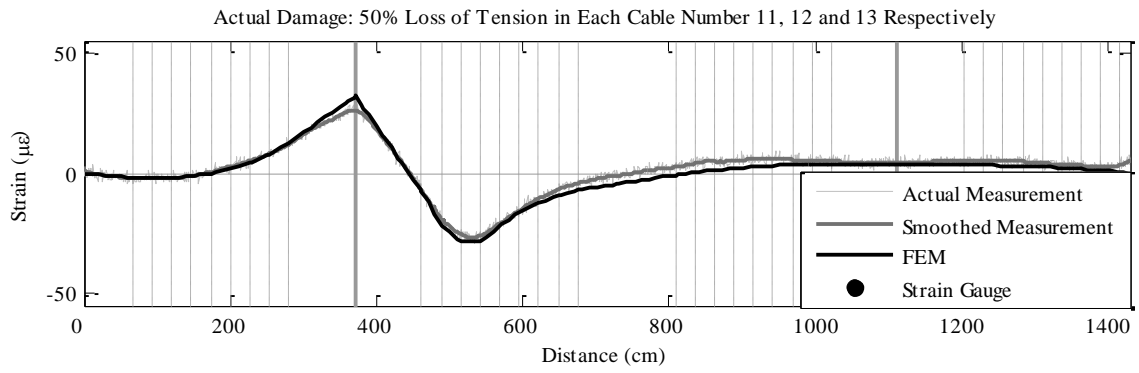Actual Damage: 30% Loss of Tension in Cable Number 4
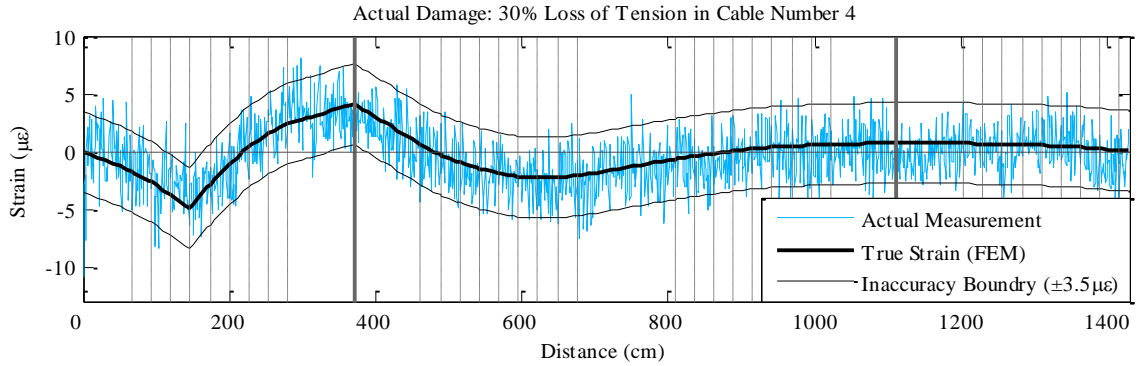
Figure 21. Evaluation of the accuracy limits for the BOTDA sensor

Due to lower inherent noise associated with localized strain sensors (Bao et al. 2015), they can provide higher resolution measurements along the bridge deck. Numerical simulation of several different damage scenarios were employed to evaluate accuracy of the proposed technique by using the localized strain sensors. Introduction of various random noise of up to 30% percent were involved in the simulations to account for severe noise in field measurements. Typical results are shown in Figure 22. Figure 22.a pertains to the change in local strains due to 10% loss in tension of each cable number 35 and 36. As shown in Figure 22.b, it is possible to detect cable tension losses as low as 10% by using a series of high-resolution discrete sensors along the bridge deck.

(a)

Actual Damage: 10% Loss of Tension in Each Cables Number 35 and 36

(b)
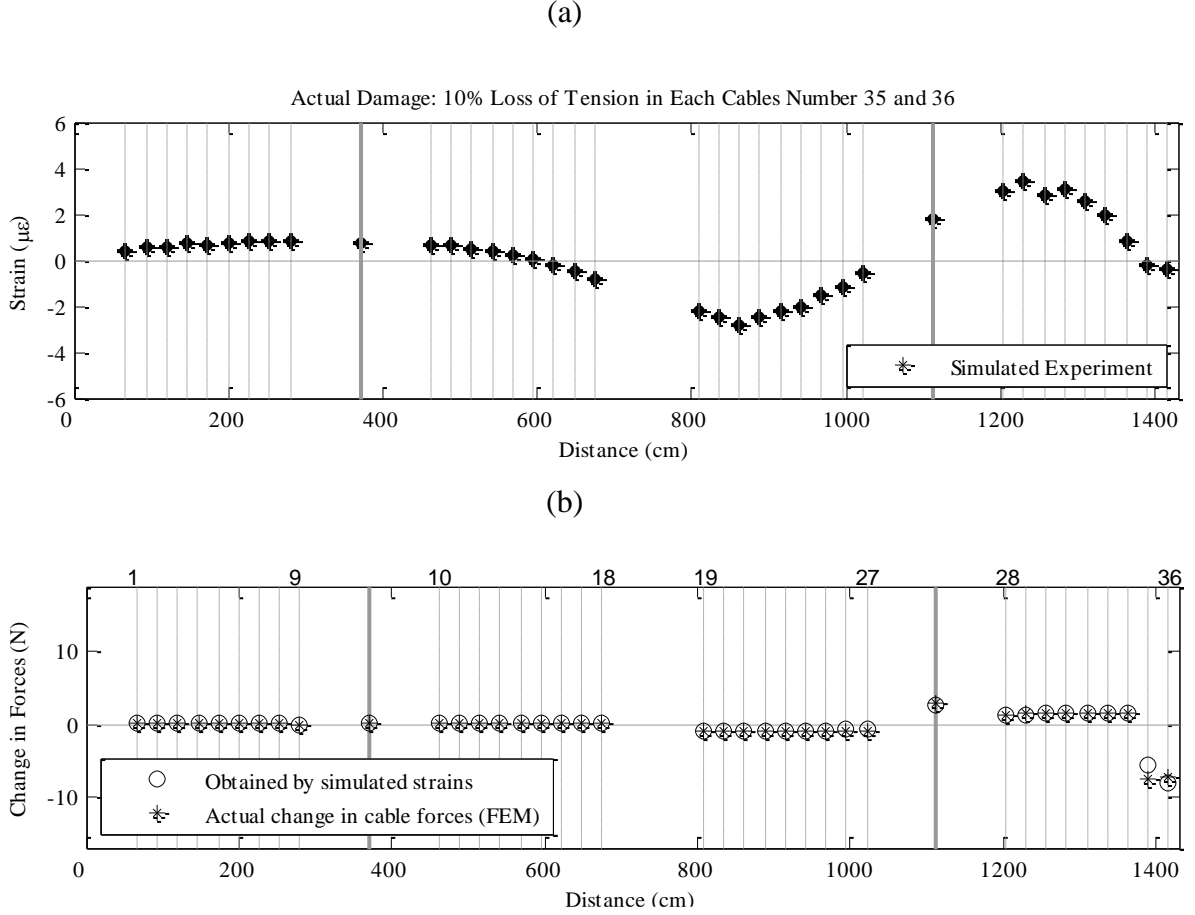
Figure 22. Dual-cable damage scenario with ten percent tension loss

3.3. Monitoring of Cable-stayed Bridges with Discrete Sensors

In the previous section, the efficiency of the proposed approach using distributed sensing was evaluated. In a similar manner, in this section the performance of the shear based formulations which utilizes discrete sensors is evaluated through both expeimentations and

59

finite element analysis.

3.3.1. Experimental Plan

The damage cases shown in Table III were employed for the evaluation of the proposed

method, both in the laboratory experiments as well as in the numerical simulations. The

objective was to test the resolution of the method in terms of the damage intensity levels,

here defined in terms of tension loss in the cables, as well as the number and location of

damaged cables detected simultaneously under various damage cases.

Table III. Damage cases considered for the evaluation of the method

Experiment Number	Damaged cable number(s)	Actual damage intensity in each cable
1	23	5%
2	18	10%
3	14	20%
4	11	30%
5	9	60%
6	4	100%
7	4 and 5	5%
8	13 and 14	10%
9	13 and 14	20%
10	14 and 23	30%
11	5 and 14	60%
12	11 and 18	100%

Accordingly, damage cases shown in Table III encompass a full range from the low level of five percent all the way to the total tension loss in the cables (100%). The locations of the damaged cables were selected in order to represent various proximities with respect to the bridge supports along the deck. Therefore, it was possible to examine the robustness of the method in terms of the affected cable location along the bridge deck. As shown in Table III, both single as well as dual cable damage scenarios were considered. Experiments were also performed for cases with damage in three cables. However, it was not possible to obtain reasonable results in these experiments, and therefore, they are not included in
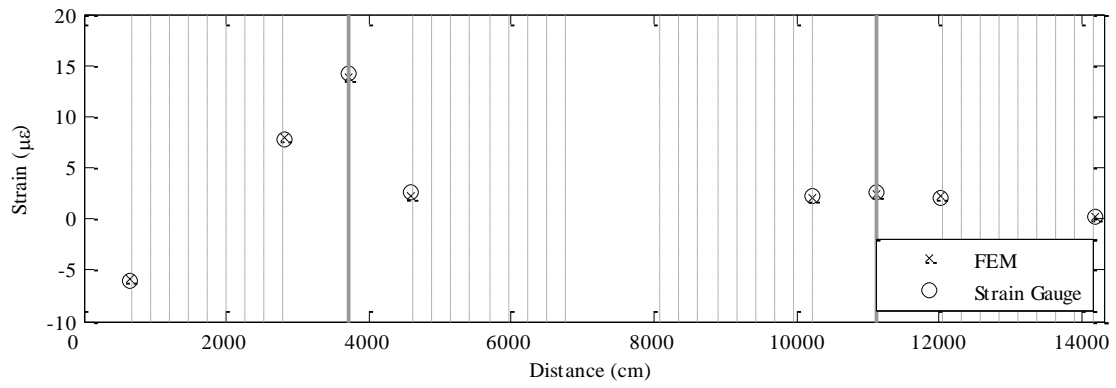
Table III.

The Finite Element Model (FEM) of the bridge was constructed using the commercial software SAP2000. An interface program was coded to compute the sensitivity matrix at each iteration step. Moreover, for each of the damage scenarios shown in Table III, the response of the numerical model was compared with the experimental strains. Frame elements were utilized for modeling the pylons and deck elements, and the cables were modeled using cable elements.

3.3.2. Experimental results

The experiments were conducted by imposing the damage scenarios shown in Table III to the model bridge by varying the tensile force in the bridge cables. Control and adjustment of cable forces was achieved by using turnbuckles at the cable anchors. As described earlier, FBG sensors were used for monitoring the change in cable forces. The required amount of change in cable forces was determined by simulating each damage scenario on the FEM of the bridge. For each damage level, the bridge deck flexural strains were measured by the strain gauges. Typical experimental and simulation results for single cable damage cases are shown in Figures 23 and 24. Figure 25 pertains to a case where two cables were damaged. Figures 23(a), 24(a), and 25(a) show the raw strain gauge outputs of the eight strain gauges along the bridge deck for the experiments number 6, 3 and 9, presented in Table III, respectively. The figures show the numerically computed strains from the

finite element simulations as well. The strains obtained by strain gauges were employed

for the detection of the change in cable forces at each one of the individual iteration steps.

Results are shown in Figures 23(b), 24(b), and 25(b). As demonstrated in Table III, the

experimental program was designed to consider the damaged cables irrespective of their

locations along the span or proximity to other cables. In Figure 23(b), the first iteration

erroneously indicates that two adjacent cables (numbers 4 and 5) were damaged. However,

subsequent iterations led to convergence towards the actual failed cable. Figures 24 and 25

pertain to single and dual-cable damage scenarios, respectively. Due to the fact that there

are low damage intensities in these two damage cases, the differences in the initial and final

iteration steps were negligible. Table IV corresponds to comparison of results between the

actual damage and those computed based on the experimental results including percentage

of error. Results shown in Table IV pertain to situations where the tension loss in the cables

is 20% or higher. As earlier shown in Table III, experiments were also performed for lower

intensity damage scenarios resulting in 5 percent and 10 percent loss in cable tension in

each of the experiments, respectively. However, the effect of lower cable tension losses on

deck strains were minute, and below the level of noise associated with the measurements.

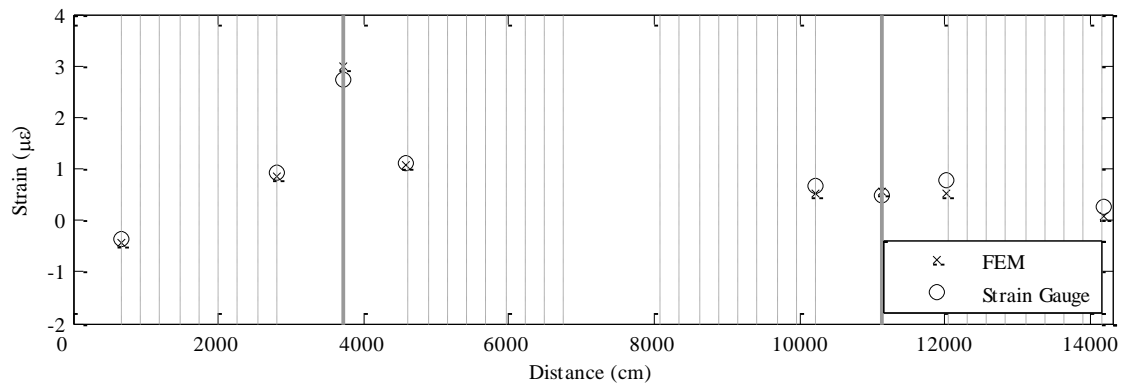These experiments did not yield satisfactory results.
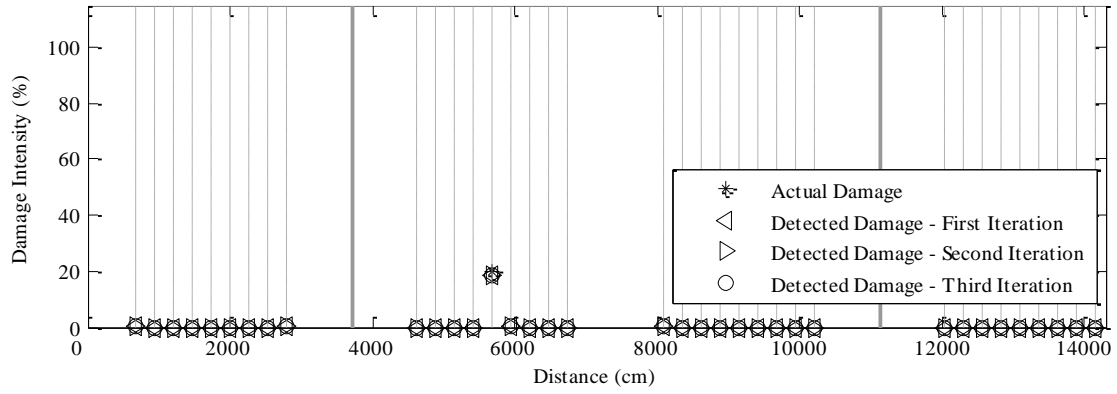
(a)
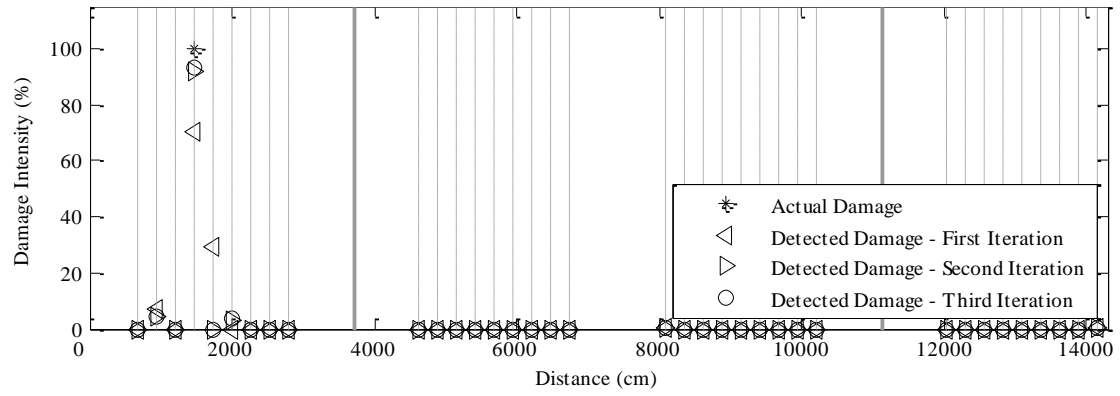
(b)

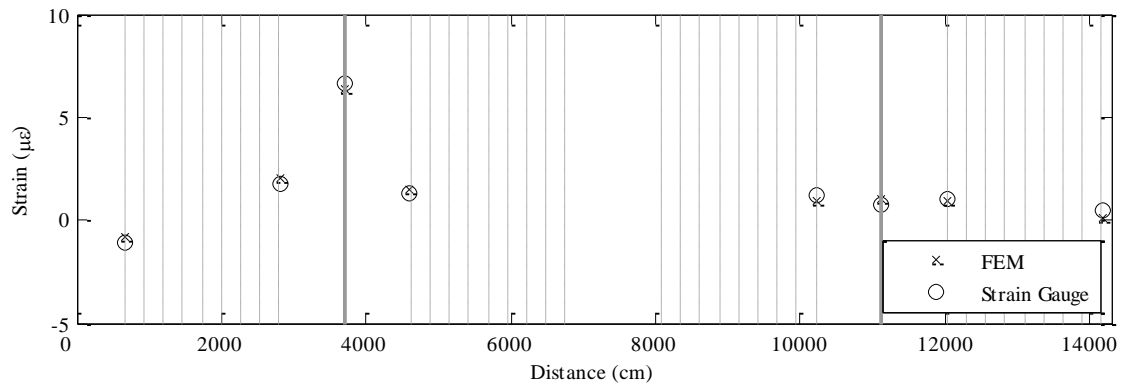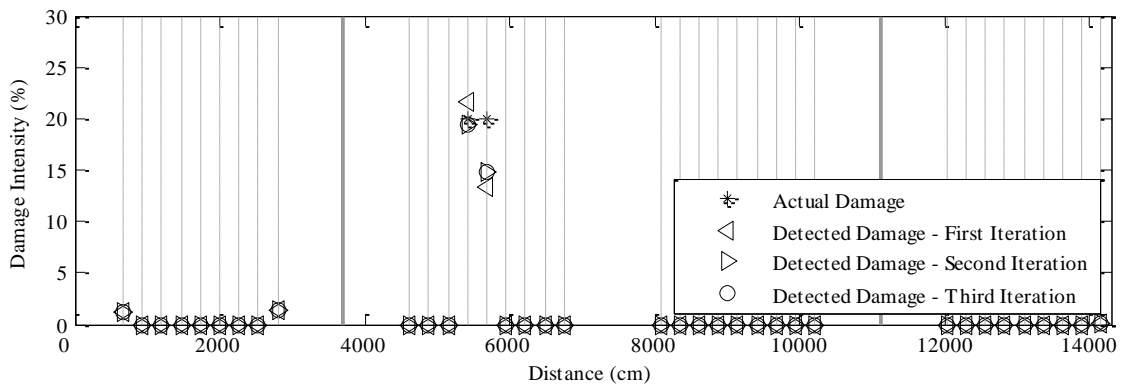**Figure 23. Single cable damage (a) cable strains, (b) detected damage**

(a)

(b)

Figure 24. Single cable damage: (a) cable strains, (b) detected damage

(a)

(b)

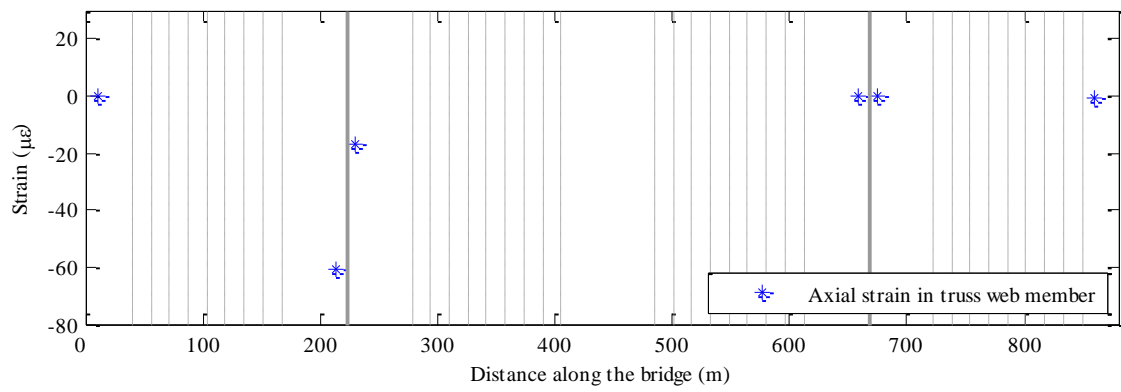**Figure 25. Dual-cable damage: (a) cable strains, (b) detected damage**

Table IV. Evaluated damage cases on the laboratory scale model bridge

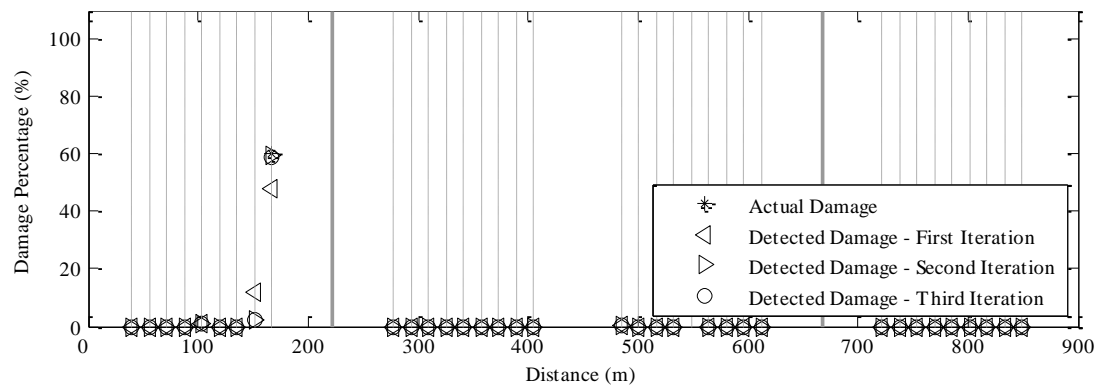| Experiment Number	Damaged cable number(s)	Actual damage intensity in each cable	Detected cables damage intensities, respectively	Relative error
1	14	20%	19.1%	4.5%
2	11	30%	29.3%	2.3%
3	9	60%	61.7%	2.8%
4	4	100%	92.1%	7.9%
5	13 and 14	20%	19% and 15%	5% and 25%
6	14 and 23	30%	24% and 32%	20% and 6.7%
7	5 and 14	60%	46% and 39%	23% and 35%
8	11 and 18	100%	91% and 77%	9% and 23%

3.3.2. Numerical Simulation Results

Following the experimental proof of concept tests, the efficiency of the proposed technique was further evaluated by numerical simulation of damage in the Dongshuimen bridge. The damage scenarios shown in Table III were simulated in the finite element model of this bridge. The simulations also involved introduction of up to five percent white noise in order to account for the field conditions. In the numerical model, the intensity of simulated noise was varied in order to examine the robustness of the approach. The simulations show that 50% tension loss in a cable adjacent to the support, for instance cable number 10, introduces 51$\mu\epsilon$ at the diagonal truss member of the nearest support. Similarly, 50% of tension loss in the furthest cable to the support, for example cable number 18, introduces 11$\mu\epsilon$ at the diagonal truss member of the nearest support. In these two damage cases, ±5%

of noise corresponds to $\pm2.5\mu\epsilon$ and $\pm0.5\mu\epsilon$, respectively, which exceeds the strain sensor

resolution of $0.1\mu\epsilon$, allowing room for environmental sources of errors (Li et al., 2004). In

the case of 10% tension loss, $\pm5\%$ of noise corresponds to $\pm0.5\mu\epsilon$ and $\pm0.1\mu\epsilon$ in the two

damage cases respectively. The simulations revealed that for noise levels above the 5%

threshold, it was not possible to acquire meaningful results. The deck-truss strains were

obtained at the locations shown in Figure 3, in order to compute the shear forces at the

bridge supports. Figures 26(a) and 27(a) pertain to the deck strains employed in the

simulations. In a manner similar to the results shown in Figures 23(b), 24(b) and 25(b),

typical results from the simulations are shown in Figures 26(b) and 27(b), which

correspond to the detected cable damage in the Dongshuimen Bridge. The computed and

actual damage scenarios for the cases considered during the simulations, including the
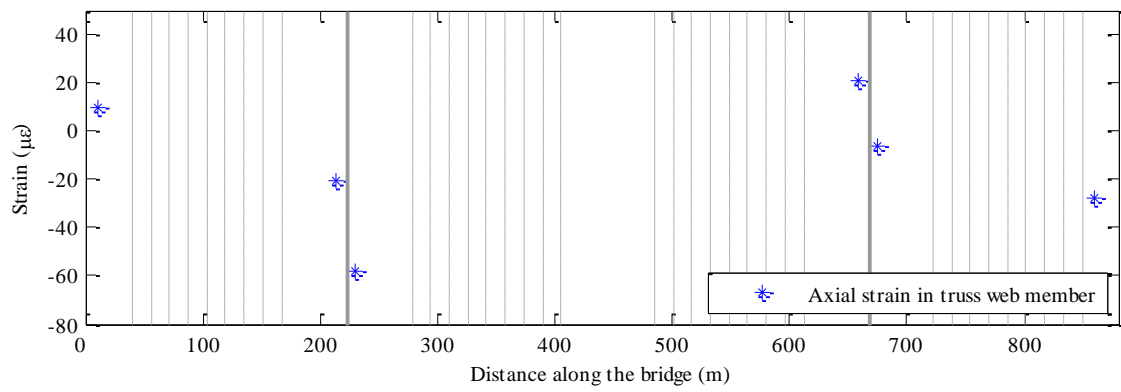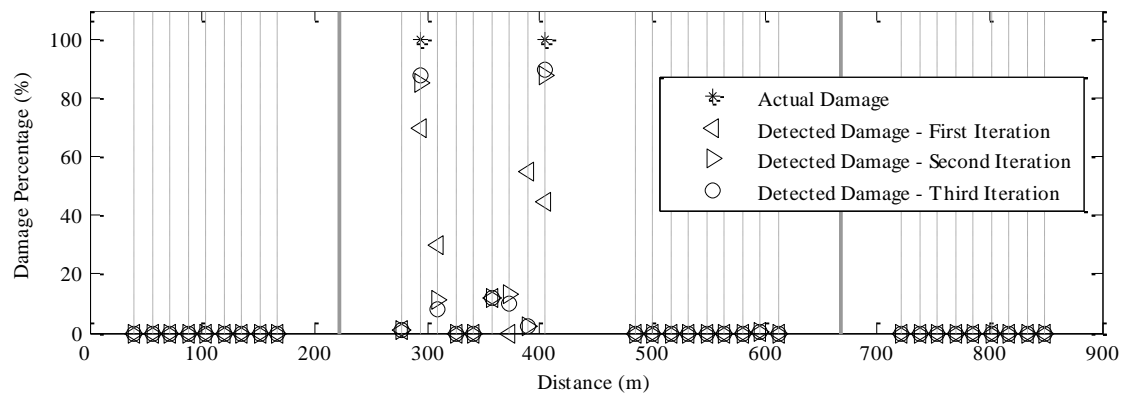
percent error are shown in Table V.

(a)

(b)

Figure 26. Single-cable damage: (a) cable strains, (b) detected damage

(a)

(b)

Figure 27. Dual-cable damage: (a) cable strains, (b) detected damage

Table V. Evaluated damage cases on actual bridge

Experiment Number	Damaged cable number(s)	Actual damage intensity in each cable	Detected cables damage intensities, respectively	Relative error
1	23	5%	5.3%	6.0%
2	18	10%	9.4%	6.0%
3	14	20%	19.0%	5.0%
4	11	30%	28.7%	4.3%
5	9	60%	58.6%	2.3%
6	4	100%	88.4%	11.6%
7	4 and 5	5%	3.8% and 5.6%	24% and 12%
8	13 and 14	10%	8.4% and 11.6%	16% and 16%
9	13 and 14	20%	16.3% and 23.4%	18% and 17%
10	14 and 23	30%	18.5% and 27.2%	38% and 9%
11	5 and 14	60%	40.3% and 46.6%	33% and 22%
12	11 and 18	100%	87% and 90.6%	13% and 9.4%

As demonstrated in Tables IV and V, in using this method, it was possible to identify the locations of the damaged cables for all the cases studied here. For cases involving damage in single cables, the percent error for quantification of the damage level was less than eight percent, except for simulation number 6 for cable number 4 in Table V, where the error between the actual and computed damage was 11.6 percent. These results also indicate that the damage quantification was more accurate for cables near the supports. The proximity of the damaged cable to one of the supports is associated with larger change in reaction at that particular support, and therefore, more accurate quantification of damage. More errors were associated in the quantification of damage in cases involving dual cables, where the

effects of redistribution of individual cable strains on the support reactions affected the computation of cable tension losses. However, as shown in Table IV, in a manner similar to the quantification of damage in single cables, the quantification errors were less pronounced for the cables near the support. This can be observed in experiment number 5, where the error due to quantification of tension loss in cable number 13 was five percent, whereas, for cable number 14, the error was twenty five percent. In experiment number 7, cables number 5 and 14 were both away from the supports and therefore, both involved larger errors. The damage quantification accuracy can be further improved by employing more strain sensors. In order to examine the relationship between the number of sensors and the accuracy of measurements, more strain sensors along the interior sections of the deck span were used in the simulation. As shown in Figure 28, in compare to the six strain sensors shown in Figure 3, the new simulations included four additional sensors for a total of ten sensors. Utilization of additional strain sensors resulted in reduction of quantification errors, as illustrated in Table VI.

Table VI. Evaluated damage cases on actual bridge

Experiment Number	Damaged cable number(s)	Actual damage intensity in each cable	Detected cables damage intensity utilizing 10 sensors	Relative error with employment of 6 sensors	Relative error with employment of 10 sensors
10	14 and 23	30%	34.5% and 34.6%	38% and 9%	15% and 15.3%
11	5 and 14	60%	68.1% and 67%	33% and 22%	13.5% and 12%
12	11 and 18	100%	97% and 96%	13% and 9.4%	3% and 4%
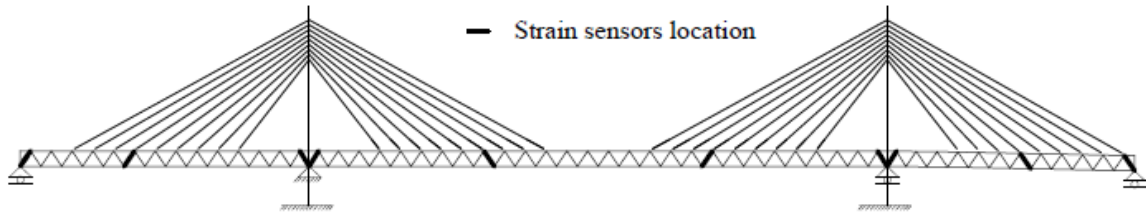
Figure 28. Employment of additional strain sensors at diagonal truss web members

In general, for all the damage scenarios studied here, three to four iterations were sufficient for convergence. The proposed method was also employed in a series of experiments involving three cables. However, the results were unsatisfactory and it was not possible to accurately detect the location of damaged cables in the bridge. The interaction of re-distributed strains involving more than two cables results in the inability of the method to detect the sources of re-distributed strains. Detection of damage in three or more cables requires increasing the number of sensors along the bridge span.

CHAPTER 4

4. FIELD IMPLEMENTATIONS

The content of this chapter was published as "Nazarian E, Ansari F, Zhang X, Taylor T (2016) Detection of Tension Loss in Cables of Cable-Stayed Bridges by Distributed Monitoring of Bridge Deck Strains. Journal of Structural Engineering, 142(6), 04016018" and "Nazarian E, Ansari F, Azari H (2015). Recursive optimization method for monitoring of tension loss in cables of cable-stayed bridges. Journal of Intelligent Material Systems and Structures, 1045389X15620043". Reproduced with permission from ASCE and Journal of Intelligent Material Systems and Structures.

In this chapter, the machine learning based approaches described in the second chapter will be evaluated on a heritage building located in Chicago. The evaluations involved both numerical simulations and actual experimentations on the building structure under study.

4.1. Heritage Building and Structural Properties

Evaluation of the method described herein was accomplished through numerical simulation and experimentation on a historical timber-framed masonry building that was built in early 20th century. The structure under consideration in this study is a historical six-story building located in Chicago, Illinois (Figure 29). The exterior of the building includes masonry columns and walls (Figure 30). The interior of the building utilizes pinned timber frames to support the gravitational loads (Figure 31).

Figure 29. The schematic view of the building under study
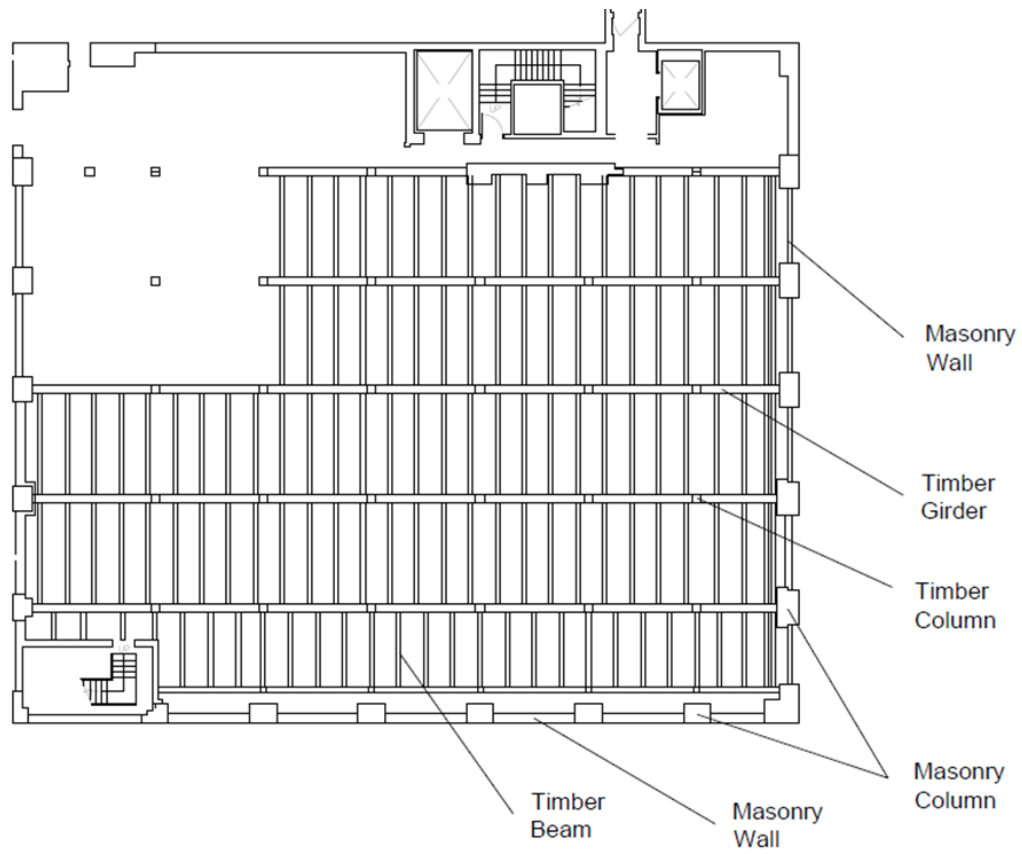
Figure 30. The structural plan of the building under study

Figure 31. Timber structural system

The gravitational loads on the floor are transferred to the simple supported timber beams, and the timber beams transfer the loads to the simple supported girders. From the girders, the loads are then transferred to the column and finally to the foundation (Figure 32). Figure 33 depicts the gravitational load path. The original plans of the building indicated that Douglas fir was used for the timber framing of the structure. The cross-sectional dimensions of the timber beams and girders were measured to be 38.1x19cm, and

38.1x38.1cm, respectively. The flooring is approximately 10cm thick. The cross-sectional dimensions of the timber columns vary at each floor. The timber columns in the basement and first floor have the largest cross-sectional dimension, 38.1x38.1cm. The dimensions of the timber columns in the second, third, fourth, fifth and six floors are 33x33cm, 33x33cm, 28x28cm, 24.1x24.1cm, 24.1x24.1cm, respectively. Similarly, the cross-sectional dimensions of the masonry columns were reduced in ascending order per floor. The dimensions of the masonry columns facing south at the sixth, fifth, fourth, third, second and first floors are approximately 117x46cm, 117x56cm, 117x66cm, 117x76cm, 117x86cm, respectively. In other words, the thickness is increased by 10cm at every lower floor.

Figure 32. Typical timber column's footing
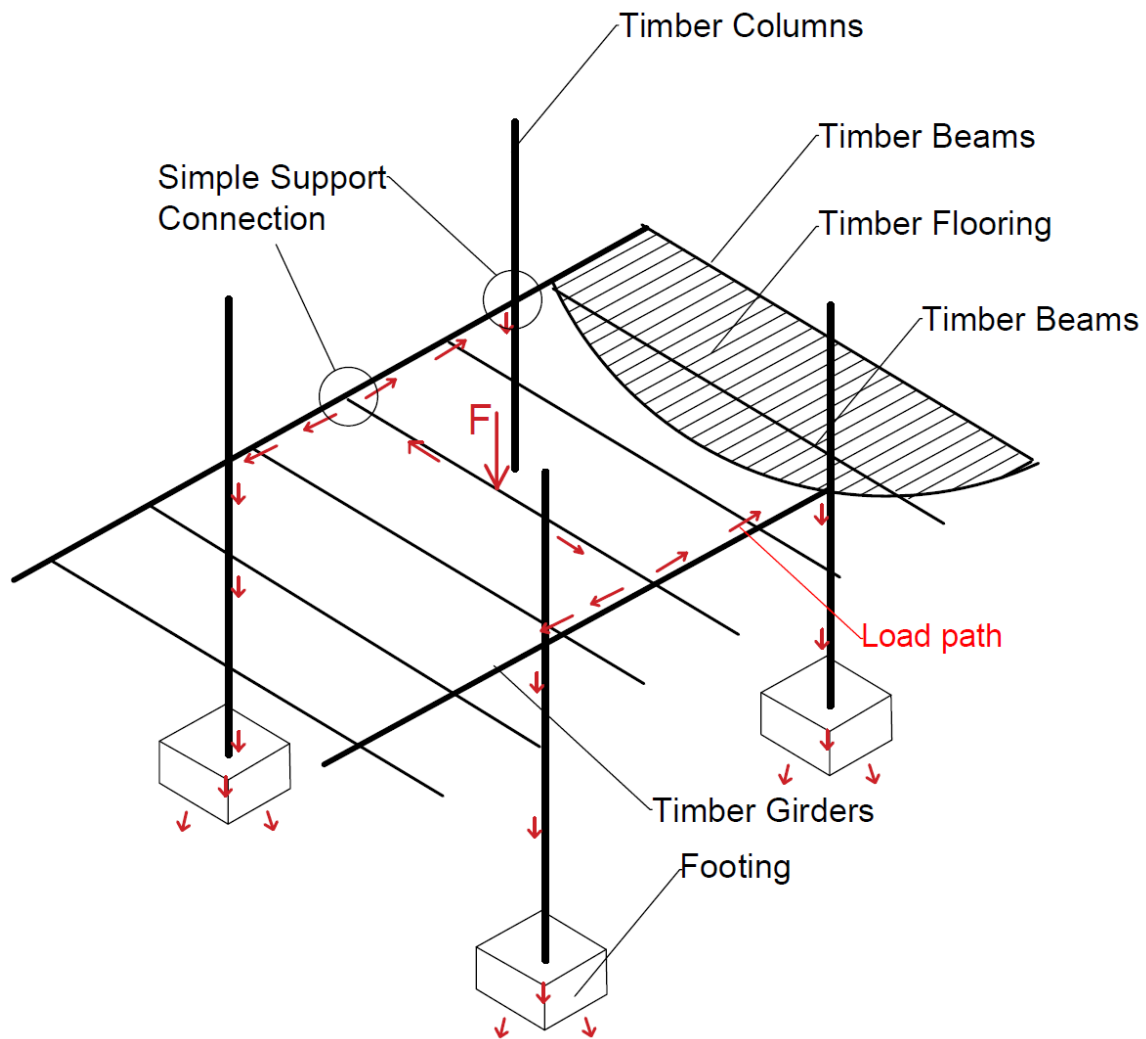
Figure 33. Structural system of the building under study

The foundation in the southeast corner of this building was substantially settled in 2015, due to nearby construction excavations. The differential settlements caused extensive cracks in the masonry elements (Figure 34 and 35). The timber framing did not get

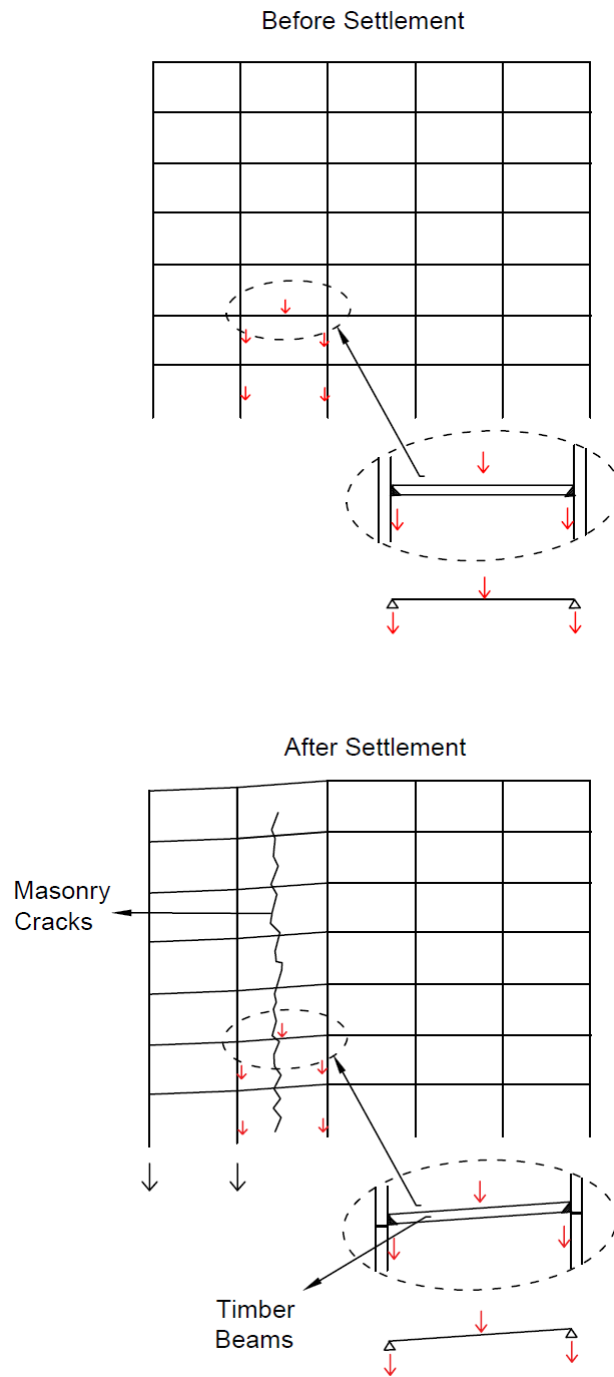damaged, since the simply supported girders were able to translate and rotate freely at the

column connections (Figure 36).

**Figure 34. Excavations adjacent to the building**

Figure 35. Typical cracks in the masonry wall as a result of differential settlements

Before Settlement

Masonry
Cracks

After Settlement

Timber
Beams

Figure 36. Displacement of timber beams due to settlement

To create the finite element model of this building, we first needed to determine the modulus of elasticity of the timber and the boundary conditions of the girders. We determined the modulus of elasticity of the timber by applying a gravitational load on multiple girders and measured their response by means of strain sensors. Figure 37 shows the experimental setup and output of a typical experiment. Fiber Optic Bragg Grating sensors were employed in the tests, which are comprised of polyimide coated optical fibers (Ansari 2007; Meng et al. 2013; Nazarian et al. 2015, 2016). The applied gravitational load at the mid-span of the girder was increased in increments to ensure the linear response of the girder. The applied load versus the monitored bending strain at the mid-span is shown in Figure 38. As it can be seen in Figure 37, only negligible bending strains were observed at the two ends of the timber beam, indicating that the girders were designed to act as simply supported beams. Based on the cross sectional dimensions of the beams, and the measured strains, the modulus of elasticity of the timber employed in the framing of the building was computed to be 15.7 GPa.
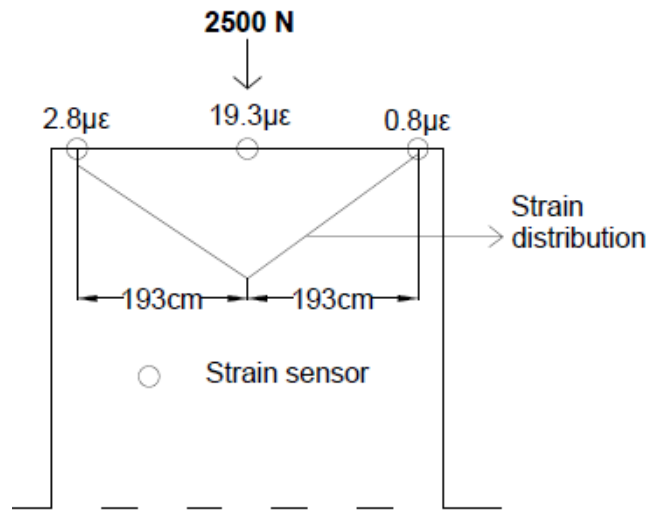
Figure 37. Gravitation loading output of a typical structural frame
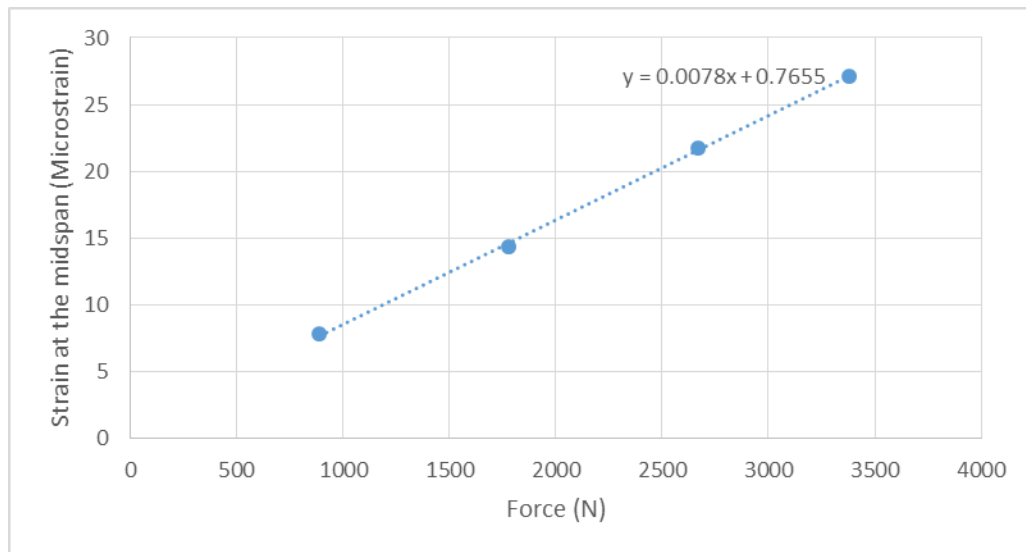
Figure 38. The imposed gravitational load versus the monitored bending strain

In a similar manner, the average modulus of elasticity of masonry was determined by application of a horizontal load to the masonry wall of the building facing south. In this case, frame number 1 of the building shown in Figure 39 was employed as a reaction element during the application of the horizontal load. Response of the masonry wall was measured by strain sensors. Figure 40.b shows the photo of the experimental setup. The experimental plan and the measured strains are shown in Figure 40.a. Two different loading configurations were examined to ensure that the same modulus of elasticity was obtained from both load tests. Since the thickness of the mortar layer and the FBG sensor are known, we determined the modulus of elasticity of the mortar and the brick by distributing the strain sensor over one and two layers of mortar as shown in Figure 41. Since the sum of the elongation of brick and mortar due to bending strain is equivalent to the elongation of the sensor (Figure 42), one can write:

$$\varepsilon_m h_m + \varepsilon_b(h_s - h_m) = h_s \varepsilon_s \tag{48}$$

Where,

$$\varepsilon_m = \frac{\sigma_s}{E_m} \tag{49}$$

$$\varepsilon_b = \frac{\sigma_s}{E_b} \tag{50}$$

ε_m is the strain in the mortar, ε_b is the strain in the brick, h_m is the thickness of the mortar,

h_s is the gauge length of the sensor, ε_s is strain output of the sensor and σ_s is the average stress along the sensor's gauge length. In this equation, h_m and h_s were measured physically (Figure 41.a), σ_s was determined by applying the loading pattern that was employed in the finite element model and obtaining the average stress at the location of strain sensor. By utilizing Equation 48 for both test scenarios (Figure 41), the modulus of elasticity of mortar and brick were obtained to be 1.77GPa, and 2.83GPa respectively. It should be noted that the masonry walls were painted. Hence, the authors have modified the photos in Figure 41.a to indicate the location of the mortar layers.
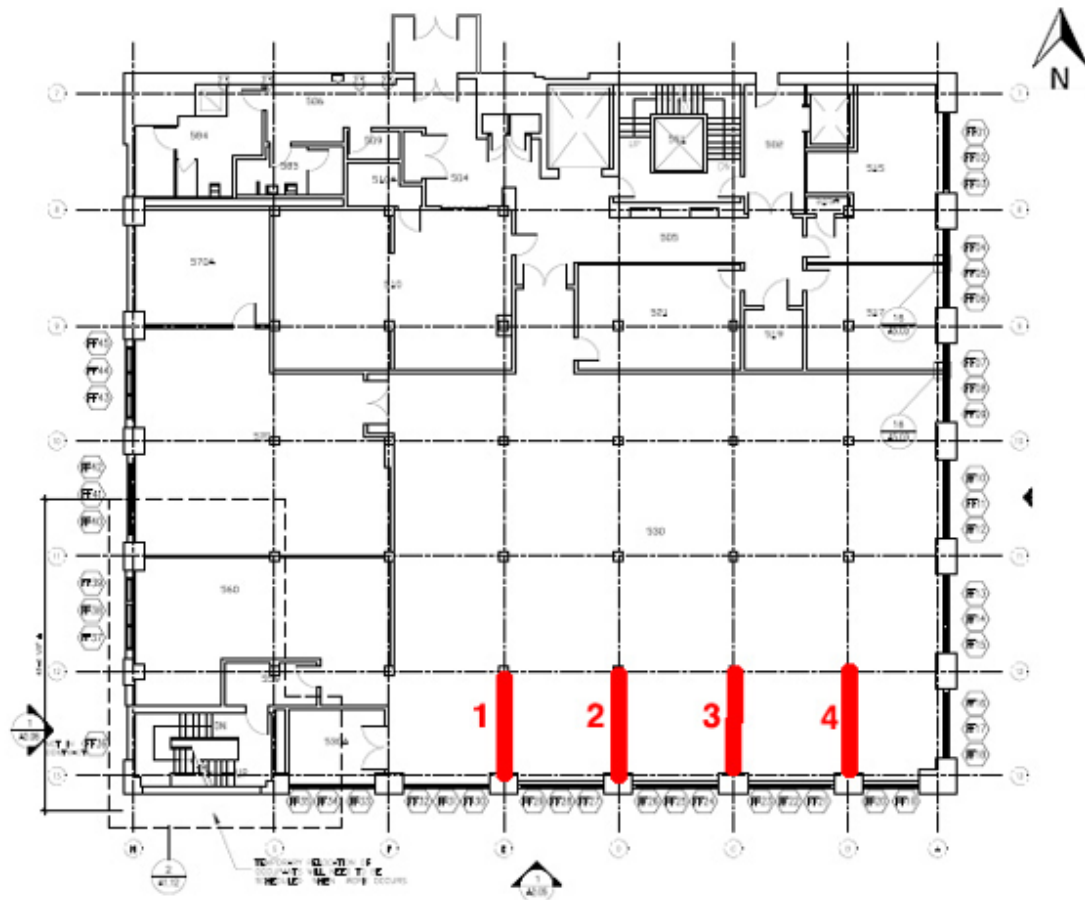
Figure 39. Structural loading location and frames numbers in the fifth floor
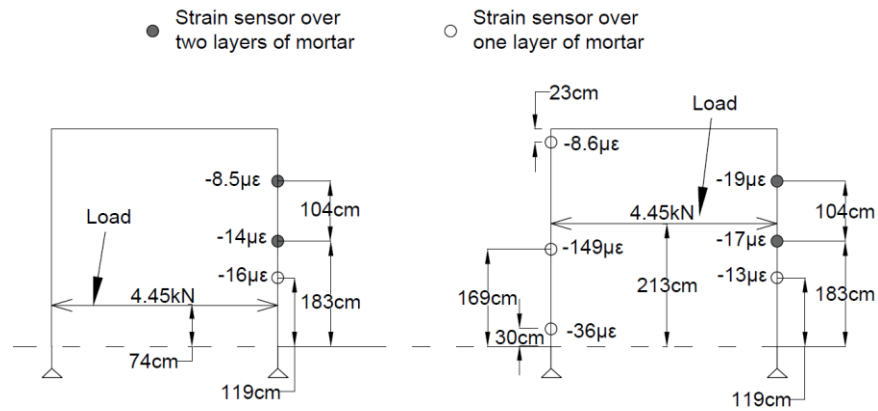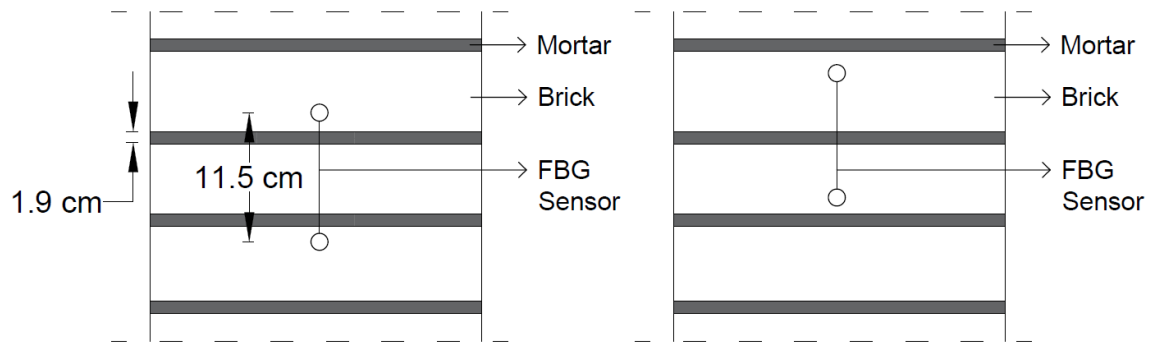
a)

b)

Figure 40. Structural loading: a) strain output; b) experimental setup

a)
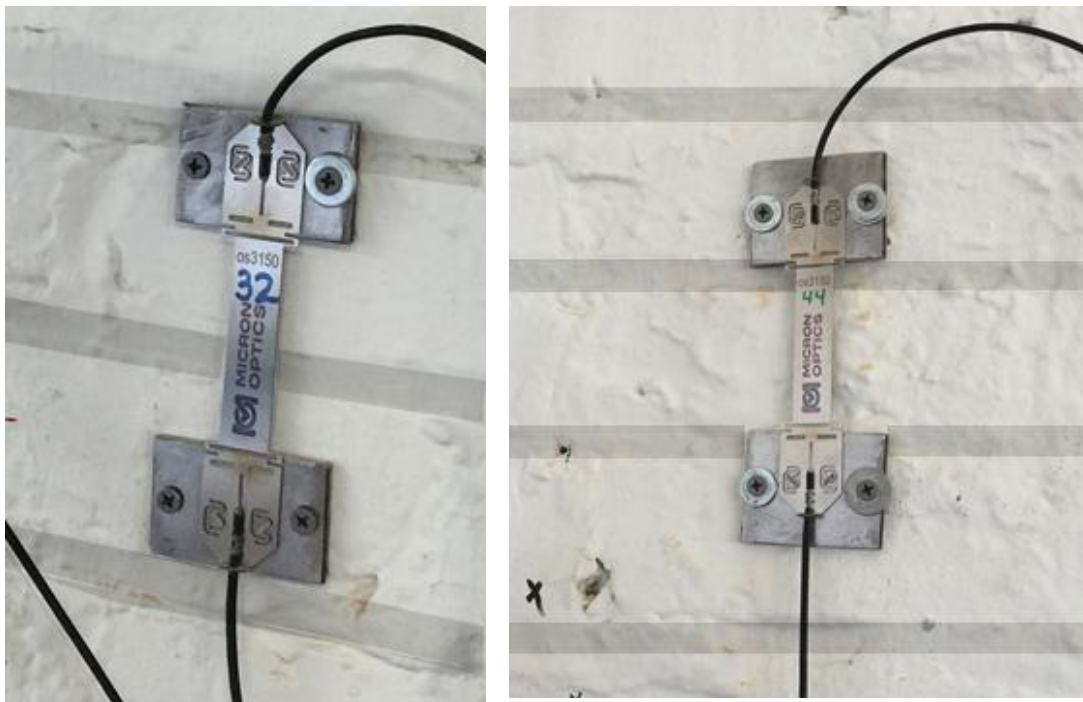
b)

Figure 41. Arrangement of strain sensors a) dimensions b) experimental setup
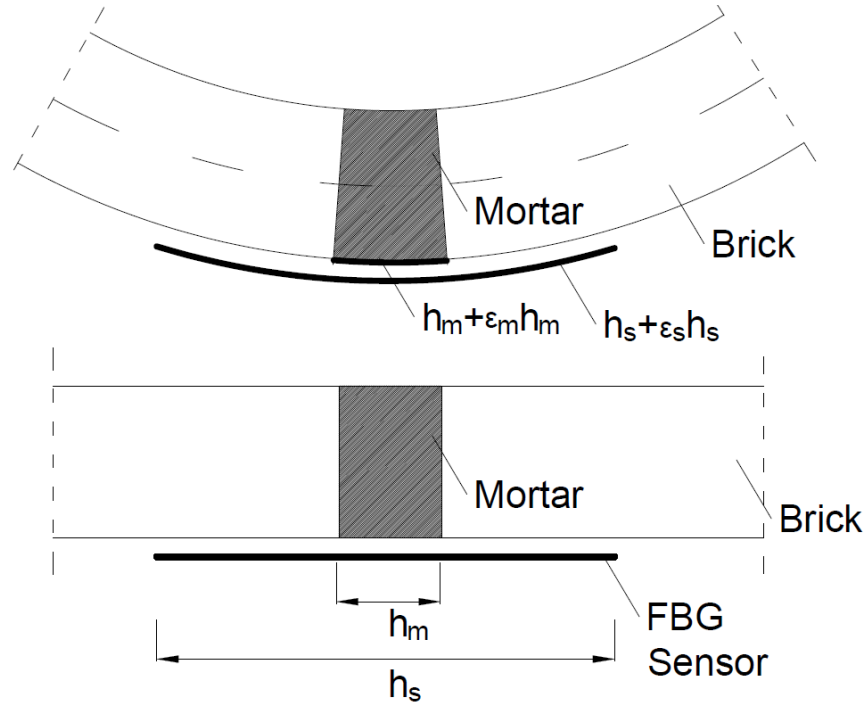
Figure 42. Strain distribution over mortar and brick layers

The Finite Element Model (FEM) of the building was constructed by using the commercial software SAP2000 (Figure 43). The walls were modeled as shell elements, and frame elements were utilized for modeling the columns, beams and girders. In training the machine learning models, all possible damage scenarios were simulated. Simulations of all the possible damage scenarios are time consuming. Hence, the simulations were automated by way of a program using C++ and employed as interface to the SAP2000 software. This approach enabled programmed reduction in the stiffnesses of structural elements for myriads of damage scenarios, and extraction of the strains from the FEM for training the

machine learning models.
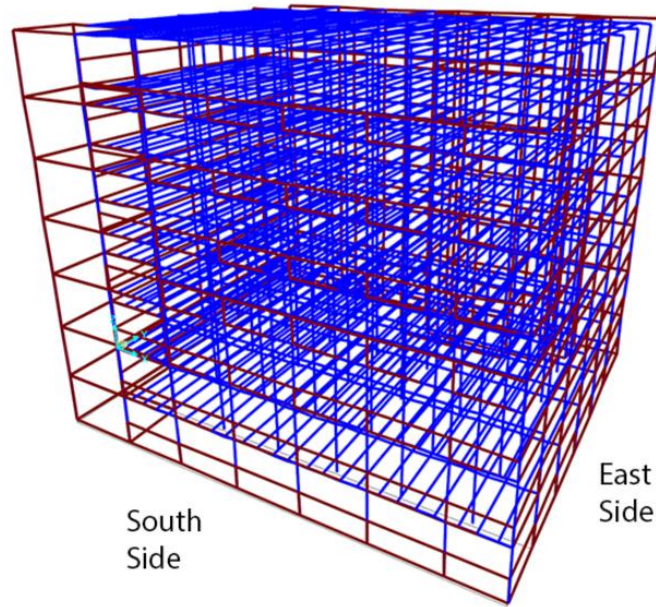
Figure 43. Finite element model (FEM) of the building

4.2. Numerical Simulation Results

The efficiency of the proposed technique was first evaluated by numerical simulation of damage in the finite element model of the building structure. We simulated multiple structural damage scenarios by reducing the stiffness of structural members on the south side of the fifth floor of the building. We then applied the loading shown in Figure 44 on frames 1 through 4 of the finite element model of the building (Figure 39). The strain responses from the simulated sensors shown in Figure 44 were acquired from the model

for utilization as input to the ML model. The sensor and loading locations were chosen so that they are identical to the experimental verification tests that are discussed in the subsequent sections of this article.

In training of the model the loading configurations shown in Figure 44 was employed for every damage scenario. The models could then be trained since both the input strains and type of damage were known. The possible damaged elements considered in this study are shown in Figure 45, which also shows the identification number for the structural elements. The lower masonry elements were excluded, because the FEM results indicated that the strains obtained by applying the load test on the fifth floor do not provide information about the integrity of the lower three floors. The upper three floors have smaller cross-sectional dimensions; hence they have a weaker capacity against horizontal load effects, such as wind loads. Testing the fifth floor provides information about the integrity of the sixth, fifth and fourth floor elements. Hence the fifth floor was chosen as the test location to evaluate the weakest sections of the building.
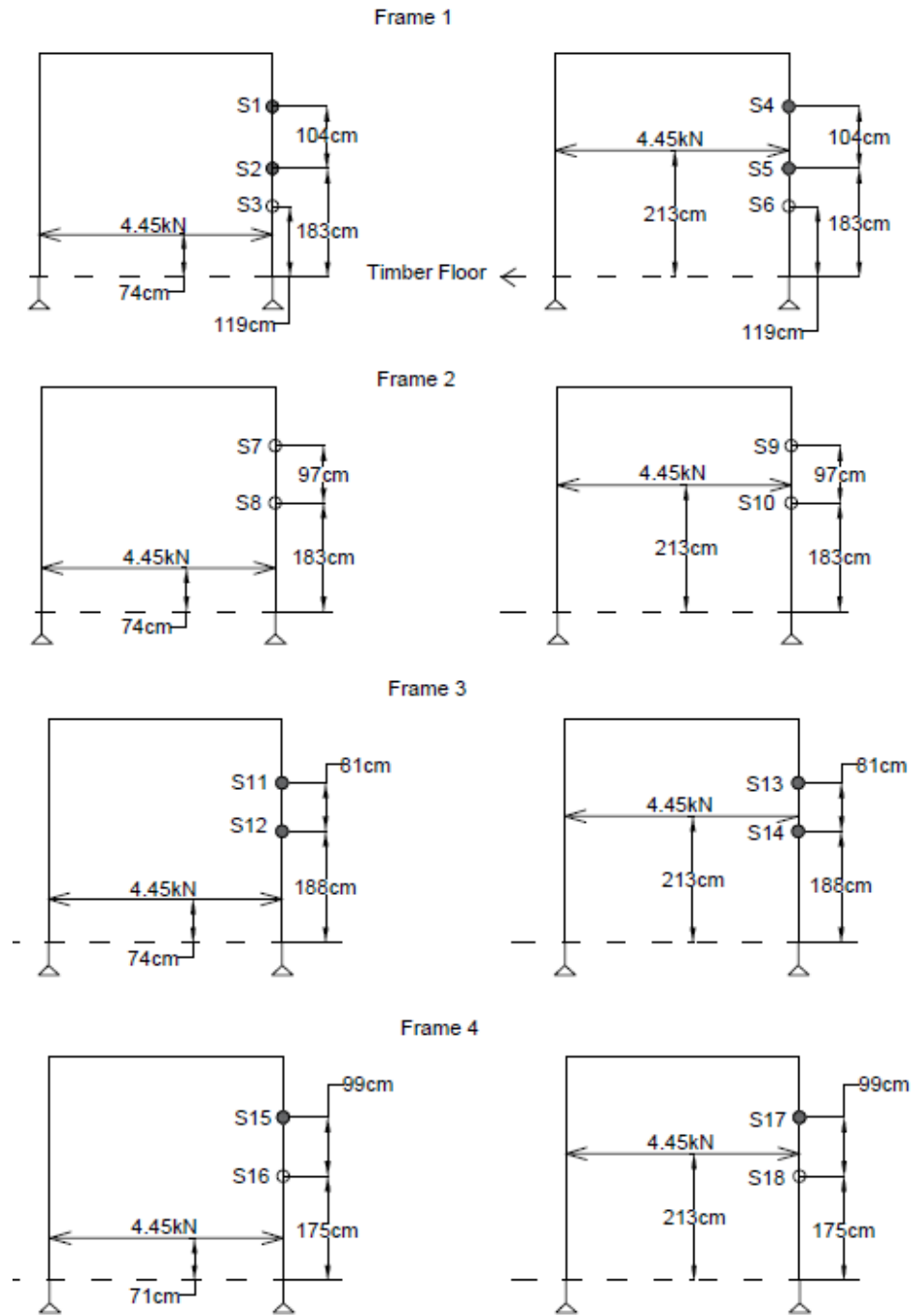
Figure 44. Load and sensor configurations on the structural frames

a)

b)

Figure 45. Possible damaged members in; a) masonry walls b) masonry columns

Sensor noise was considered in training the model by simulating 1000 different versions of white noise of up to 10% of the extracted strains. Table VII shows the prediction accuracy of the SVM, NN and GNB approaches for various noise levels. Table VII demonstrates that NN model provides the highest accuracy. Furthermore, it can be seen that when a noise level of 10% is used, the prediction accuracy drops significantly for all the three approaches. Hence, in this study, a noise level of up to 8% was used for training of the ML model. The prediction accuracy was determined by k-fold cross validation

method with a k factor of 10 (Kohavi, 1995).

Table VII. Prediction Accuracy

Noise Level (%)	SVM Prediction Accuracy	NN Prediction Accuracy	GNB Prediction Accuracy
2	97%	98%	98%
4	96%	96%	96%
6	91%	93%	92%
8	86%	90%	88%
10	79%	86%	83%

The damage scenarios shown in Table VIII were simulated as stiffness loss for evaluations of the three ML methods. For instance, the first row indicates that 20% of stiffness loss was simulated in element number 19 (Figure 45). The changes in strains due to the loading configurations in Figure 44 were then extracted from the finite element model. Table IX shows the strain output of the simulated model due to the proposed loading configuration including 8% noise to account for field conditions. These strain results were then employed in the machine learning method to determine the location and intensity of damage in structural members. Utilizing the ML model, the location of the structural members subjected to stiffness losses were determined accurately using all three methods. However, the damage intensities were determined with an error. The damage intensities and the relative errors using the three ML models are listed in Table X.

Table VIII. Simulated Damage

Element number	Damage intensity
19	20
10	10
11	15
14	70

Table IX. Simulated strain sensors output

Sensor ID	Strain ($\mu\varepsilon$)	Sensor ID	Strain ($\mu\varepsilon$)
S1	-8.5	S10	-18
S2	-14	S11	-12
S3	-16	S12	-15
S4	-19	S13	-22
S5	-17	S14	-20
S6	-13	S15	-10
S7	-10	S16	-19
S8	-14	S17	-21
S9	-21	S18	-28

Table X. Percentage of error

Element Number	Actual Damage Intensity	Detected Damage Intensity (NN)	Relative Error (%)	Detected Damage Intensity (SVM)	Relative Error (%)	Detected Damage Intensity (GNB)	Relative Error (%)
19	20	18	-10	18	-10	18	-10
10	10	10	0	11	10	10	0
11	15	16	7	14	-7	16	7
14	70	64	-9	62	-11	63	-10

According to the results shown in Table X, the three methodologies were capable of determining the intensity of damage. NN provided the best results and SVM yielded larger errors. SVM predicted the structural damages with a maximum relative error of 11%.

4.3. Experimental Results

Following the numerical proof of concept tests, the proposed technique was further applied to determine the damage by testing the structure. The experiments were conducted by imposing horizontal loads in the same manner as in the numerical model. A typical structural loading experimental setup is shown in Figure 46.

Figure 46. Experimental setup for structural loading

In a similar manner to section 3, Fiber Optic Bragg Grating sensors were employed in the tests. A hydraulic jack with pressure gauge was utilized to apply the load between the columns. The loading increased to 11.1 KN, in 2.22 kN increments. The strain response was recorded at various force increments. Load tests and the location of strain sensors mimicked those in the numerical simulations described earlier (Figure 44). Table XI shows the raw strain sensor data for the eighteen strain gauges employed in the experiments.

Table XI. Strain sensors output

| Sensor ID	Strain (με)	Sensor ID	Strain (με)
S1	-8.5	S10	-17
S2	-14	S11	-10
S3	-16	S12	-35
S4	-19	S13	-28
S5	-17	S14	-48
S6	-13	S15	-10
S7	-8	S16	-27
S8	-15	S17	-38
S9	-18	S18	-38

The strains shown in Table XI were used as input to the ML models. The intensity and location of the damaged members were then obtained. Figure 47, 48 and 49 depict the predicted loss of stiffness in the structural members using NN, SVM and GNB methods, respectively. The x-axis pertains to the element numbers depicted in Figure 45. The stiffness losses determined by NN model, the model with highest prediction accuracy, were simulated in the finite element model of the building to confirm that the result of the simulated sensors and experimental strains are in agreement. Table XII compares the strains of the experiments and the strains obtained using the corresponding simulated structure. The results indicate that, except for member S7 and S17, the relative error between the strain levels was below 15%. The strain sensor readings for S7 and S17 are the lowest in compare to other sensors. Hence, they are significantly affected by the inherent sensor noises. This creates higher chance of error.
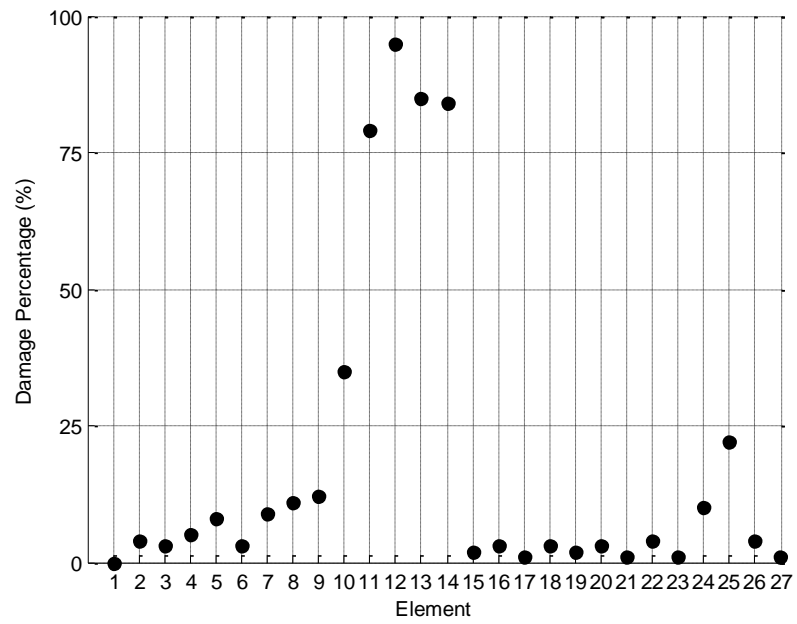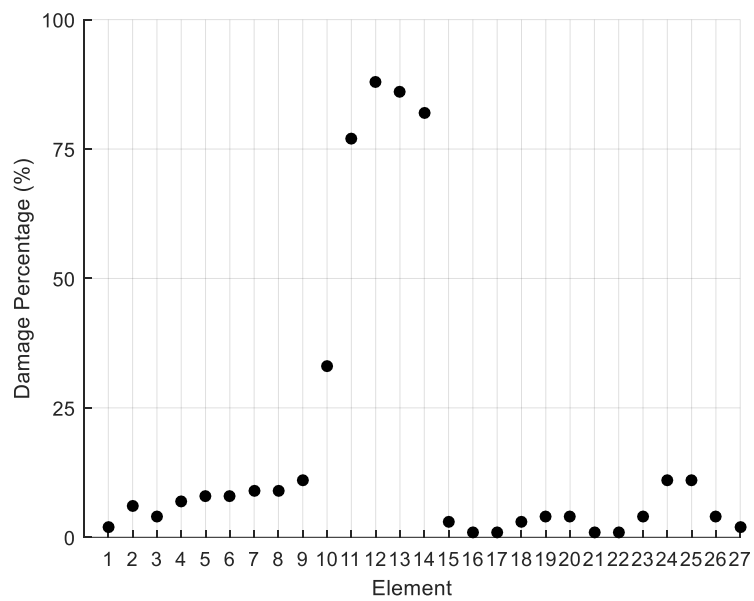
Figure 47. Detected percentage of damage in structural elements using NN
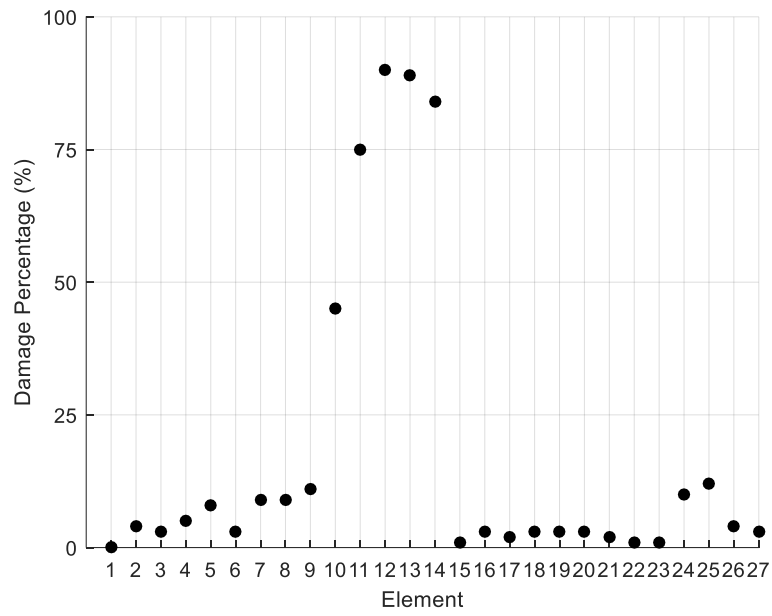
Figure 48. Detected percentage of damage in structural elements using SVM

Figure 49. Detected percentage of damage in structural elements using GNB

Table XII. Strain sensors output

Actual Experiments		Simulaitons	Relative
Sensor ID	Strain (με)	Strain (με)	Error (%)
S1	-8.5	-9.7	14
S2	-14	-14.8	2
S3	-16	-18.0	13
S4	-19	-20.8	10
S5	-17	-19	12
S6	-13	-13.3	2
S7	-8	-10.0	25
S8	-15	-17.3	15
S9	-18	-19.0	5
S10	-17	-18.3	8
S11	-10	-11.3	13
S12	-35	-36.5	4
S13	-28	-29.2	4
S14	-48	-49.2	2
S15	-10	-12.2	22
S16	-27	-27.2	1
S17	-38	-39.6	4
S18	-38	-38.6	2

CHAPTER 5

5. CONCLUSIONS

The content of this chapter was published as "Nazarian E, Ansari F, Zhang X, Taylor T (2016) Detection of Tension Loss in Cables of Cable-Stayed Bridges by Distributed Monitoring of Bridge Deck Strains. Journal of Structural Engineering, 142(6), 04016018" and "Nazarian E, Ansari F, Azari H (2015). Recursive optimization method for monitoring of tension loss in cables of cable-stayed bridges. Journal of Intelligent Material Systems and Structures, 1045389X15620043". Reproduced with permission from ASCE and Journal of Intelligent Material Systems and Structures.

As increasing proportion of infrastructures are exceeding their design life, and therefore, safety evaluation of such structures is becoming more important. In this thesis, methodologies were developed for damage assessment by means of fiber optic and electrical sensors. The developed methodologies utilize mathematical, probabilistic and machine learning approaches to quantify and locate damages in building and cable-stayed structures.

The objective of the work described in the first chapter pertained to the development of an efficient method for detecting the cables that had either totally or partially lost their tensile force carrying capacities by distributed monitoring of the deck strains alone. A distributed sensing technology, BOTDA, was used to obtain the change of strain along the bridge deck. The methodology was evaluated through numerical simulations and actual experiments. The results indicated that the methodology is capable of detecting the cables that have lost over 30% of their tensile force.

The second chapter pertained to establishment of a structural health monitoring strategy based on discrete sensors to determine the tension losses in the cables of cable-stayed bridges. Point sensors were used to determine the change in shear forces adjacent to the supports. The proposed mathematical methodology then detected the location and intensity of damage in the cables using a recursive optimization technique based on finite element analysis. In a similar manner to the first chapter, the efficiency of the methodology was evaluated using numerical analysis and actual experimentations. The results indicated that the method introduced herein, is capable of identifying the location and intensity of damages that involve up to two damaged cables.

The work described in the third chapter pertains to structural health monitoring of building structures using a machine-learning based approach. The objective of this chapter was to develop a methodology to determine the location and the level of damage by applying selective load tests on the structural frames. The proposed approach utilized three machine learning approaches, namely: Neural Networks, Support Vector Machines, and Gaussian Naïve Bayes. The methodology was first evaluated by simulating damage in the finite element model of the building. The simulation results indicated that the proposed methodology is capable of recognizing the structural damages with 86% prediction accuracy, if the sensors noise level is within 8%. Furthermore, the efficiency of the approach was evaluated by implementing load tests on a six-story heritage building which was subjected to differential settlements.

CITED LITERATURE

Abeykoon D, Kawarai K, Yamaguchi H, Matsumoto Y, Yoshioka T (2015) Experimental-Analytical Framework For Damping Change-Based Structural Health Monitoring Of Bridges

Ansari F (2007) Practical Implementation of Optical Fiber Sensors in Civil Structural Health Monitoring. Journal of Intelligent Material Systems and Structures 18(8): 879–889.

Bao T, Babanajad S K, Taylor T, and Ansari F (2015) Generalized Method and Monitoring Technique for Shear-Strain-Based Bridge Weigh-in-Motion. J. Bridge. Eng., 04015029.

Bao X (2009) Optical fiber sensors based on Brillouin scattering Opt. Photonics News, 20(9), 40–46.

Bungey J H (1980) The validity of ultrasonic pulse velocity testing of in-place concrete for strength NDT International, Volume 13, Issue 6

Camara A, Astiz M, and Ye A (2014) Fundamental Mode Estimation for Modern Cable-Stayed Bridges Considering the Tower Flexibility. J. Bridge Eng. 19(6), 04014015.

Cao M, Sha G, Gao Y, Ostachowicz W (2016) Structural Damage Identification Using Damping: A Compendium of Uses and Features. Smart Materials and Structures.

Carpinteri A, Lacidogna G (2006) Damage monitoring of an historical masonry building by the acoustic emission technique. Materials and Structures, 39(2), 161-167.

Cho S, Yim J, Shin S, Jung H, Yun C, Wang, M (2013) Comparative Field Study of Cable Tension Measurement for a Cable-Stayed Bridge. J. Bridge Eng., 18(8), 748–757.

Christen R, Bergamini A, Motavalli M (2003) Three-dimensional localization of defects in stay cables using magnetic flux leakage methods J. Nondestruct. Eval., 22 (3), 93– 101.

Dilek U (2007) Ultrasonic Pulse Velocity in Nondestructive Evaluation of Low Quality and Damaged Concrete and Masonry Construction J. Perform. Constr. Facil., 10.1061/(ASCE)0887-3828(2007)21:5(337), 337-344.

Feng X, Wu W, Meng D, Ansari F, Zhou J (2016) Distributed monitoring method for upheaval buckling in subsea pipelines with Brillouin optical time-domain analysis sensors. Advances in Structural Engineering, 1369433216659990.

Feng X, Zhang X, Sun C, Motamedi M, Ansari F (2014) Stationary Wavelet Transform Method for Distributed Detection of Damage by Fiber-Optic Sensors J. Eng. Mech., 140(4), 04013004.

Feng X, Zhou J, Sun C, Zhang X, and Ansari F (2013) Theoretical and Experimental Investigations into Crack Detection with BOTDR-Distributed Fiber Optic Sensors. J. Eng. Mech., 139(12), 1797–1807.

Fricker S, Vogel (2007) Site installation and testing of a continuous acoustic monitoring Constr. Build. Mater. 21 (3), 501-510.

Furey T S, Cristianini N, Duffy N, Bednarski D W, Schummer M, Haussler D (2000) Support vector machine classification and validation of cancer tissue samples using microarray expression data. Bioinformatics, 16(10), 906-914.

Glisic B, Inaudi D (2010) Distributed Fiber-Optic Sensing and Integrity Monitoring. Transportation. Research Record: Journal of the Transportation Research Board, 2150(1), 96-102.

Gorokhovich Y, Doocy S, Voustianiouk A, Small C (2010). Assessment of Mortar and

Brick Strength in Earthquake-Affected Structures in Peru Using a Schmidt Hammer. J. Perform. Constr. Facil., 10.1061/(ASCE)CF.1943-5509.0000120, 634-640.

Hagan M T, Menhaj M B (1994) Training feedforward networks with the Marquardt algorithm. IEEE transactions on Neural Networks, 5(6), 989-993.

Harris G H, Sabnis G (2011) Structural Modeling and Experimental Techniques, 2nd Ed.

Hegab H (1986) Energy analysis of cable-stayed bridges. J. Struct. Eng., 112(5), 1182 – 1195.

Hegab H (1988) Parametric Investigation of Cable-Stayed Bridges. J. Struct. Eng. 114(8), 1917–1928.

Hippert H S, Pedreira C E, Souza R C (2001) Neural networks for short-term load forecasting: A review and evaluation. IEEE Transactions on power systems, 16(1), 44-55.

Horiguchi T, Shimizu K, Kurashima T, Tateda M, Koyamada Y (1995). Development of a distributed sensing technology using Brillouin scattering. J. Lightwave Technol., 13(7), 1296–1302.

Horiguchi T, Tateda M (1989) Tensile strain dependence of Brillouin frequency shift in silica optical fibers. Photon. Technol. Lett., 1(5), 107–108.

Hotate K, Tanaka M (2001) Correlation-based continuous-wave technique for optical fiber distributed strain measurement using Brillouin scattering with an cm-order spatial resolution. IEICE Trans. Electron., E84-C(12), 1823–1828.

Ispir M, Demir C, Ilki A, Kumbasar N (2010) Material Characterization of the Historical Unreinforced Masonry Akaretler Row Houses in Istanbul. J. Mater. Civ. Eng., 10.1061/(ASCE)MT.1943-5533.0000071, 702-713.

John G H, Langley P (1995) Estimating continuous distributions in Bayesian classifiers. In Proceedings of the Eleventh conference on Uncertainty in artificial intelligence (pp. 338-345). Morgan Kaufmann Publishers Inc.

Kang S G, Kang D H, Kim C G (2009) Real-time monitoring of transverse thermal strain of carbon fiber reinforced composites under long-term space environment using fiber optic sensors NDT&E Int., 42(5), 361-368.

Kim B H, Park T (2007) Estimation of cable tension force using the frequency-based system identification method. J. Sound Vib., 304, 660–676.

Kim S W, Jeon B G, Kim N S, Park J C (2013) Vision-based monitoring system for evaluating cable tensile forces on a cable-stayed bridge. Structural Health Monitoring, 12(5-6), 440-456.

Kishida K, Zhang H, Li C-H, Guzik A, Suzuki H, Wu Z (2005) Diagnostic of corrosion based thinning in steam pipelines by means of Neubrescope high precision optical fiber sensing system. Proc., Int. The 5th International Workshop on Structural Health Monitoring, Stanford University, Stanford, CA, 1363-1370.

Kohavi R (1995) A study of cross-validation and bootstrap for accuracy estimation and model selection. In Ijcai (Vol. 14, No. 2, pp. 1137-1145).

Kouris L A S, Kappos A J (2012) Detailed and simplified non-linear models for timber-framed masonry structures. Journal of Cultural Heritage, 13(1), 47-58

Lanza di Scalea F, Rizzo P, and Seible F (2003) Stress measurement and defect detection in steel strands by guided stress waves. J. Mater. Civil. Eng. 15(3), 219-227.

114

Li D, Zhou Z, and Ou J (2011) Development and sensing properties study of FRP-FBG smart cable for bridge health monitoring applications. Measurement, 44, 722-729.

Li H, Ou J, Zhou Z (2009) Application of optical fiber bragg grating sensing technology-based smart stay cables. Opt. Laser Eng., 47, 1077-1084.

Li H N, Li D S, Song G B (2004) Recent applications of fiber optic sensors to health monitoring in civil engineering. Engineering structures, 26(11), 1647-1657.

Mehrabi B (2006) In-Service Evaluation of Cable-Stayed Bridges, Overview of Available Methods, and Findings. J. Bridge. Eng., 11(6), 716–724.

Meng D, Ansari F (2013) Damped fiber optic low-frequency tiltmeter for real-time monitoring of structural displacements. Measurement Science and Technology 24, no. 12.

Milgram J, Cheriet M, Sabourin R (2006) "One Against One" or "One Against All": Which One is Better for Handwriting Recognition with SVMs?. In Tenth International Workshop on Frontiers in Handwriting Recognition. Suvisoft.

Motamedi M H, Feng X, Zhang X, Sun C, Ansari F (2013). Quantitative investigation in distributed sensing of structural defects with Brillouin optical time domain reflectometry. J. Intell. Mater. Syst. Struct., 24 (10), 1187–1196.

Nazarian E, Ansari F, Azari H (2015). Recursive optimization method for monitoring of tension loss in cables of cable-stayed bridges. Journal of Intelligent Material Systems and Structures, 1045389X15620043.

Nazarian E, Ansari F, Zhang X, Taylor T (2016) Detection of Tension Loss in Cables of Cable-Stayed Bridges by Distributed Monitoring of Bridge Deck Strains. Journal of Structural Engineering, 142(6), 04016018.

Park J, Park J, Cho J (2011) Estimation of Error Factors in Concrete Cable-Stayed Structures with Sensitivity of Creep. J. Struct. Eng. 137(12), 1451–1459.

Podolny W (1976) Construction and design of cable-stayed bridges. Wiley-Interscience, New York, N.Y.

Potenza F, Federici F, Lepidi M, Gattulli V, Graziosi F, Colarieti A (2015) Long-term structural monitoring of the damaged Basilica S. Maria di Collemaggio through a low-cost

wireless sensor network. Journal of Civil Structural Health Monitoring, 5(5), 655-676.

Ren W X, Chen G, Hu W (2005) Empirical formulas to estimate cable tension by cable fundamental frequency. Struct. Eng. Mech., 20(3), 363–380.

Ren W X, De Roeck G (2002). Structural damage identification using modal data II: Test verification. J. Struct. Eng. , 128 (1), 96–104.

Russell J C, Lardner T J (1998) Experimental determination of frequencies and tension for elastic cables. J. Eng. Mech. ASCE., 124, 1067–1072.

Sun Z K, Li G M, Geng S H (2013) Study on stayed-cable health monitoring. In: Intelligence Computation and Evolutionary Computation, Berlin, Germany, 7 July 2012, pp. 1091-1098. Berlin: Springer Berlin Heidelberg.

Talebinejad I, Fischer C, Ansari F (2011) Numerical evaluation of vibration based methods for damage assessment of cable stayed bridges. Computer-Aided Civil and Infrastructure Engineering, 26(3), 239–51.

SAP2000 [Computer software]. Computers and Structures, Inc., Walnut Creek, CA.

Sun Z K, Li G M, and Geng S H (2013) Study on stayed-cable health monitoring. Proc., Intelligence Computation and Evolutionary Computation, AISC, Berlin, 1091-1098.

Shaji T, Somayaji S, Mathews M (2000) Ultrasonic Pulse Velocity Technique for Inspection and Evaluation of Timber. J. Mater. Civ. Eng., 10.1061/(ASCE)0899-1561(2000)12:2(180), 180-185.

Soyoz S, Taciroglu E, Orakcal K, Nigbor R, Skolnik D, Lus H, Safak E (2013) Ambient and Forced Vibration Testing of a Reinforced Concrete Building before and after Its Seismic Retrofitting. J. Struct. Eng., 10.1061/(ASCE)ST.1943-541X.0000568, 1741-1752.

Stubbs N, Osegueda R A (1990) Global non-destructive damage evaluation in solids. Int. J. Anal. Exp. Modal Anal. , 5 (2), 67–80.

Stubbs N, Kim J T (1996) Damage localization in structures without baseline modal parameters. AIAA J. , 34 (8), 1644–1649.

Tong S, Koller D (2001) Support vector machine active learning with applications to text classification. Journal of machine learning research, 2(Nov), 45-66.

Yamauchi Y, Guzik A, Kishida K, Li C-H (2007) A study of the stability, reliability, and accuracy of Neubrescope-based pipe thinning detection system Proc., Int. The 3rd international conference on structural health monitoring of intelligent infrastructure, Vancouver, BC.

Zarafshan A, Ansari F, Taylor T (2014) Field tests and verification of damping calculation methods for operating highway bridges. Journal of Civil Structural Health Monitoring, 4(2), 99-105.

APPENDICES

Appendix A - Permissions from JIMSS

Appendix B - With permission from ASCE

On Aug 2, 2016, at 1:52 PM, PERMISSIONS <permissions@asce.org> wrote:

Dear Ebrahim,

Permission is changed so that your thesis can be 30% of your new work.

Thanks,

Joann

On Aug 2, 2016, at 9:24 AM, PERMISSIONS <permissions@asce.org> wrote:

Dear Ebrahim,

Permission is granted for you to reuse your paper "Detection of Tension Loss in Cables of Cable-Stayed Bridges by Distributed Monitoring of Bridge Deck Strains" in your my PhD dissertation/thesis, under the condition that it makes up 25% of the new work.

A full credit line must be added to the material being reprinted. For reuse in non-ASCE publications, add the words "With permission from ASCE" to your source citation. For Intranet posting, add the following additional notice: "This material may be downloaded for personal use only. Any other use requires prior permission of the American Society of Civil Engineers."

Regards,

Joann

Joann Fogleson
Manager, Product and Subscription Services
American Society of Civil Engineers

VITA

NAME   EBRAHIM NAZARIAN

EDUCATION   Ph.D. Civil Engineering
                University of Illinois at Chicago, Chicago, IL
                May 2017

                M.Sc. Computer Science
                University of Illinois at Chicago, Chicago, IL
                May 2017

                B.S. Civil Engineering
                Budapest University of Technology and Economics,
                Budapest, Hungary, June 2012

TEACHING   University of Illinois at Chicago
                Teaching Assistant
                2013-17

PROFESSIONAL   University of Illinois at Chicago
                Research Assistant
                2012-2016

PUBLICATION   Nazarian, E., Ansari, F., Zhang, X., & Taylor, T. (2016).
                Detection of Tension Loss in Cables of Cable-Stayed
                Bridges by Distributed Monitoring of Bridge Deck Strains.
                Journal of Structural Engineering, 142(6), 04016018.

                Nazarian, E., Ansari, F., & Azari, H. (2015). Recursive
                optimization method for monitoring of tension loss in cables
                of cable-stayed bridges. Journal of Intelligent Material
                Systems and Structures, 1045389X15620043.